Secretory Vesicle Clustering in Fungal Filamentous Cells Does Not Require Directional Growth

Patrícia Silva, Charles Puerner, Agnese Seminara, Martine Bassilana, Robert Arkowitz

▶ **To cite this version:**

Patrícia Silva, Charles Puerner, Agnese Seminara, Martine Bassilana, Robert Arkowitz. Secretory Vesicle Clustering in Fungal Filamentous Cells Does Not Require Directional Growth. Cell Reports, 2019, 28 (8), pp.2231-2245.e5. 10.1016/j.celrep.2019.07.062 . hal-03101911

HAL Id: hal-03101911
https://hal.science/hal-03101911

Submitted on 7 Jan 2021

HAL is a multi-disciplinary open access archive for the deposit and dissemination of scientific research documents, whether they are published or not. The documents may come from teaching and research institutions in France or abroad, or from public or private research centers.

L'archive ouverte pluridisciplinaire **HAL**, est destinée au dépôt et à la diffusion de documents scientifiques de niveau recherche, publiés ou non, émanant des établissements d'enseignement et de recherche français ou étrangers, des laboratoires publics ou privés.

Article

Cell Reports

Secretory Vesicle Clustering in Fungal Filamentous Cells Does Not Require Directional Growth

Graphical Abstract

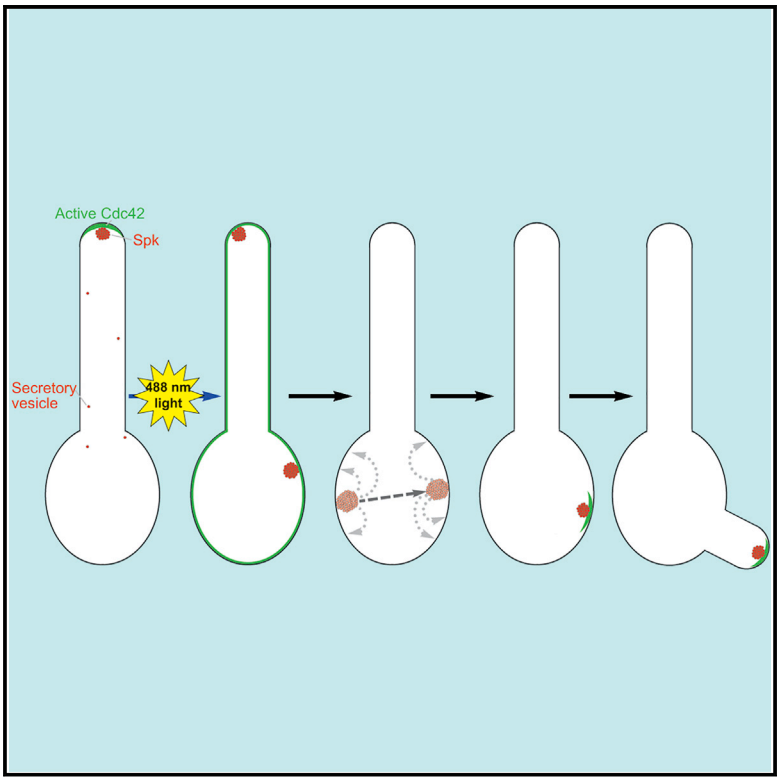

Authors

Patrícia M. Silva, Charles Puerner, Agnese Seminara, Martine Bassilana, Robert A. Arkowitz

Correspondence

arkowitz@unice.fr

In Brief

Silva et al. use light-dependent plasma membrane recruitment of active Cdc42 to reset polarity in asymmetric filamentous fungal cells. This transient increase in plasma membrane active Cdc42 disrupted membrane traffic and resulted in the formation of a striking *de novo* secretory vesicle cluster, in the absence of directional growth.

Highlights

- Photo-recruitment of active Cdc42 over the plasma membrane resets growth
- Transient increase of active Cdc42 at the plasma membrane disrupts membrane traffic
- Increase in plasma membrane active Cdc42 results in *de novo* secretory vesicle cluster
- Secretory vesicle clustering can occur in the absence of directional growth

Silva et al., 2019, Cell Reports *28*, 2231–2245
August 20, 2019 © 2019 The Author(s).
https://doi.org/10.1016/j.celrep.2019.07.062

CellPress

Cell Reports
Article

OPEN ACCESS
CellPress

Secretory Vesicle Clustering in Fungal Filamentous Cells Does Not Require Directional Growth

Patrícia M. Silva,[1] Charles Puerner,[1] Agnese Seminara,[2] Martine Bassilana,[1] and Robert A. Arkowitz[1,3,*]
[1]Université Côte d'Azur, CNRS, INSERM, Institute of Biology Valrose (iBV), Parc Valrose, Nice, France
[2]Université Côte d'Azur, CNRS, Institute Physics of Nice (INPHYNI), Ave. J. Vallot, Nice, France
[3]Lead Contact
*Correspondence: arkowitz@unice.fr
https://doi.org/10.1016/j.celrep.2019.07.062

SUMMARY

During symmetry breaking, the highly conserved Rho GTPase Cdc42 becomes stabilized at a defined site via an amplification process. However, little is known about how a new polarity site is established in an already asymmetric cell—a critical process in a changing environment. The human fungal pathogen *Candida albicans* switches from budding to filamentous growth in response to external cues, a transition controlled by Cdc42. Here, we have used optogenetic manipulation of cell polarity to reset growth in asymmetric filamentous *C. albicans* cells. We show that increasing the level of active Cdc42 on the plasma membrane results in disruption of the exocyst subunit Sec3 localization and a striking *de novo* clustering of secretory vesicles. This new cluster of secretory vesicles is highly dynamic, moving by hops and jumps, until a new growth site is established. Our results reveal that secretory vesicle clustering can occur in the absence of directional growth.

INTRODUCTION

Highly polarized growth in a range of elongated cell types, including fungal hyphae (Riquelme, 2013; Riquelme and Sánchez-León, 2014; Virag and Harris, 2006), plant pollen tubes (Bibeau et al., 2018; Bou Daher and Geitmann, 2011; Bove et al., 2008), and neurons (Denker et al., 2011; Milovanovic and De Camilli, 2017; Mukherjee et al., 2010) requires a specific cellular organization to overcome long distances. In these elongated cells, clusters of vesicles are typically observed just behind the growing cell tip and thought to provide a reservoir of material necessary for rapid cellular extension or synaptic activity. In *Saccharomyces cerevisiae,* such a cluster of vesicles also appears to be present in elongated pseudohyphal cells (Kim and Rose, 2015) and shmoos (Chapa-Y-Lazo et al., 2011), yet has not been observed in budding cells. In filamentous fungi, including *Neurospora crassa* and *Ashbya gossypii*, a number of studies have revealed that this structure, referred to as the Spitzenkörper (Spk), depends on and maintains growth (Brunswik, 1924; Girbardt, 1957, 1969; Grove and Bracker, 1970; López-Franco and Bracker, 1996; Reynaga-Peña et al., 1997; Riquelme, 2013; Riquelme and Sánchez-León, 2014; Virag and Harris, 2006). In *Candida albicans*, disruption of the actin cytoskeleton (Crampin et al., 2005; Jones and Sudbery, 2010), as well as mutants that perturb secretion, i.e., *sec3* and *sso2*, disrupt the Spk (Bernardo et al., 2014; Li et al., 2007). Together these results strongly suggest that this cluster of vesicles is a build-up resulting from limiting fusion with the plasma membrane and is intimately associated with cell growth.

Cell polarity is a fundamental process that is not fixed but rather is dynamic, allowing cells to readjust to their environment in response to a range of temporal and spatial cues. In both model yeasts *S. cerevisiae* and *Schizosaccharomyces pombe*, the active form of the highly conserved Rho GTPase Cdc42 accumulates at a unique, presumptive growth site in symmetrical, unpolarized cells (Bendezú and Martin, 2011; Bendezú et al., 2015; Butty et al., 2002; Das et al., 2009; Gallo Castro and Martin, 2018; Gulli et al., 2000; Howell et al., 2012; Jaquenoud and Peter, 2000; Kelly and Nurse, 2011; Ozbudak et al., 2005; Smith et al., 2013). This patch or cap of activated Cdc42 ultimately results in polarized growth by promoting the activation and/or recruitment of a range of effector proteins, which have critical roles in cytoskeleton organization and membrane traffic (Chiou et al., 2017). Polarization in the absence of established landmarks is thought to be the result of feedback mechanisms that amplify small differences in active Cdc42 levels via reaction-diffusion mechanisms, actin-dependent transport, membrane extraction, and differential lateral diffusion (Freisinger et al., 2013; Goryachev and Leda, 2017; Kuo et al., 2014; Martin, 2015; Witte et al., 2017; Woods and Lew, 2019; Wu et al., 2015; Wu and Lew, 2013). Recently, optogenetic recruitment of either the Bem1 scaffold protein or the Cdc42 unique guanine nucleotide exchange factor (GEF), Cdc24, was shown to be sufficient to bias the position of the polarization site in budding yeast (Witte et al., 2017).

Cdc42 is also critical for filamentous growth in a range of fungi, including pathogenic species. This GTPase has been shown to control directional growth in *N. crassa* germ tubes (Lichius et al., 2014), and deletion mutants have severe morphological

This is an open access article under the CC BY-NC-ND license (http://creativecommons.org/licenses/by-nc-nd/4.0/).

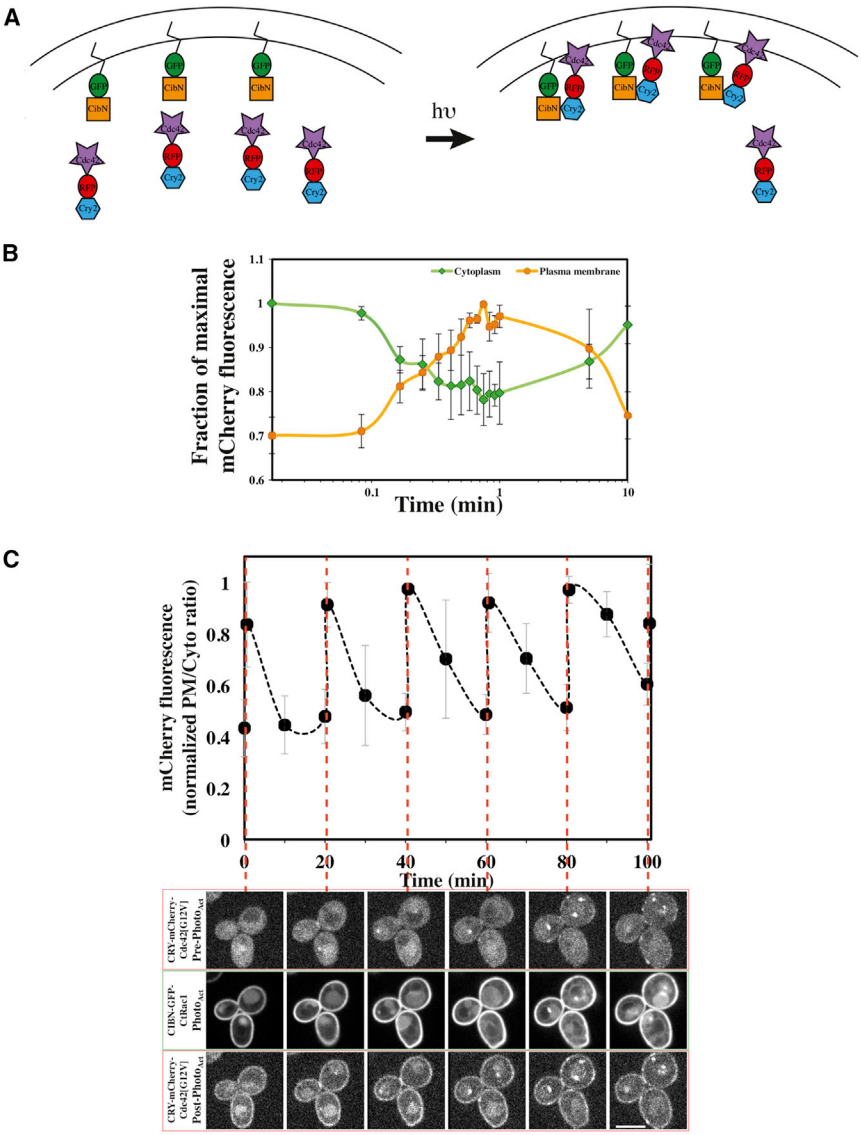

Figure 1. Rapid Recruitment of Active Cdc42 to the Plasma Membrane

(A) Schematic of optogenetic system for recruitment of active Cdc42 to the plasma membrane in *C. albicans*.

(B) Recruitment of Cdc42•GTP to the plasma membrane occurs concomitant with depletion from the cytoplasm. A strain expressing CibN-GFP-Ct_{Rac1} and Cry2-mCh-Cdc42[G12V]$_{cyto}$ was incubated on agar pads at 30°C, and the entire field of view was exposed to a 300-ms, 488-nm, 2.5-mW pulse immediately after the initial time point. The mean signals from a region of interest (ROI) of the cytoplasm or plasma membrane were quantified (n = 3) and maximum signals were normalized to 1; the average and standard deviation are shown.

(C) Cdc42•GTP can be recruited to the plasma membrane multiple times. Strain was incubated on agar pads as in Figure 1B and similarly exposed to 488 nm light every 20 min; image acquisition order was 561 nm (top row), 488 nm (middle row) and 561 nm (bottom) excitation. Signals were quantified as in Figure 1B and the mean plasma membrane to cytoplasm ratio calculated, with the maximum normalized to 1; the average and standard deviation are shown. Scale bar, 5 μm.

defects (Araujo-Palomares et al., 2011). In *Aspergillus nidulans*, mutants lacking *CDC42* exhibited defects in hyphal polarity, although the organization of the microtubule and actin cytoskeleton and the apical vesicle cluster known as the Spk were not affected (Virag et al., 2007). In the human fungal pathogen *C. albicans*, Cdc42 is required for filamentous growth, with mutants that have reduced levels of this GTPase unable to form hyphae and specific Cdc42 point mutants exhibiting defects in the yeast to hyphal transition (Bassilana et al., 2003; Ushinsky et al., 2002; VandenBerg et al., 2004). A dramatic redistribution of active Cdc42 has been observed at the incipient germ tube in *C. albicans*, with a 10-fold increase in local concentration (Corvest et al., 2013). In *C. albicans* germ tubes, the Ras-like GTPase Rsr1 is important for the tight localization of active Cdc42 at the apex (Pulver et al., 2013). Expression of a constitutively active GTP-bound form of Cdc42 is lethal in *C. albicans* (Ushinsky et al., 2002), and conditional expression of this activated mutant in hyphal cells resulted in cell swelling and reduced or altered polarity (Brand et al., 2014; Court and Sudbery, 2007).

To investigate how a new polarized growth site occurs in an asymmetric cell, we have used optogenetic tools to recruit the key GTPase Cdc42 to the cortex in *C. albicans* filamentous cells. Here, we show that photo-recruitment of active Cdc42 all over the plasma membrane resets growth and results in a striking *de novo* cluster of secretory vesicles, which is highly dynamic, moving by hops and jumps, until a new growth site is subsequently established. Our results reveal that clustering of secretory vesicles can occur in the absence of directional growth.

RESULTS

Photo-Recruitment of Active Cdc42 Disrupts Polarized Growth

To investigate cell polarization in asymmetric cells, we established optogenetic tools, based on *Arabidopsis thaliana* cryptochromes (Kennedy et al., 2010), to recruit the key regulator of polarity Cdc42 all over the cortex in *C. albicans* cells. Specifically, we co-expressed membrane-tethered CibN (CibN-GFP-Ct_{Rac1}) with Cry2-mCh fused to a constitutively active Cdc42 mutant lacking its C-terminal membrane-targeting prenylation sequence (Cry2-mCh-Cdc42[G12V]$_{cyto}$) (Figure 1A). Cells co-expressing both fusions grew normally in the dark and the mutated

version of Cdc42 was quantitatively recruited to the plasma membrane (Figure 1B). A single pulse of 488-nm light (over the entire field of view), identical to the levels and times used for a GFP image, was sufficient to recruit active Cdc42 to the plasma membrane, with maximal recruitment observed after ~1 min, concomitant with depletion from the cytosol. Within 10 min of maximal plasma membrane recruitment, there was a decrease in plasma membrane signal (to pre-photoactivation levels) and a concomitant increase in cytoplasmic signal. Figure 1C shows that this fusion protein, which could be repeatedly recruited, was observed over the entire plasma membrane.

We next examined whether photo-recruitment of active Cdc42 perturbs cell growth. Recruitment of active Cdc42 dramatically perturbed budding growth, compared to control cells (Figure 2A). Measurements of the bud and mother cell size indicated that recruitment of active Cdc42 largely blocks polarized growth (Figure 2B)—the bud volume increased by on average only 2.6-fold following four photoactivation pulses, compared to 33-fold in the absence of Cdc42 recruitment. Nonetheless, we did observe non-polar growth, as unbudded and budded cells increased in overall size (compare cell sizes in Figure 1C at 0 and 100 min and Figure 2A at 0 and 80 min), indicating that plasma membrane recruitment of constitutively active Cdc42 specifically blocks polarized growth.

In cells that had begun to filament upon induction with serum, light-dependent recruitment of active Cdc42 blocked filament extension. Subsequently, new filamentous growth emerged more than 20 min after the last photoactivation pulse when the Cry2 fusion was no longer detectable at the cortex (Figures 1C and S1A). There was no correlation between the location of plasma-membrane-recruited active Cdc42 (over the entire plasma membrane with occasional clusters) and the new growth site (Figure S1B). As indicated above, photoactivation consisted of a 488-nm pulse identical to that used for a GFP image, which we have previously shown has no effect on filamentous growth (Ghugtyal et al., 2015; Labbaoui et al., 2017). Furthermore, addition of a mutation (Thr at position 35 in the effector loop changed to Ala) shown to disrupt active Cdc42 binding to its effectors (Davis et al., 1998; Gladfelter et al., 2001; Ottilie et al., 1995; Peter et al., 1996; Zheng et al., 1994) and plasma membrane recruitment of the resulting fusion (Cdc42[G12V,T35A]$_{cyto}$) did not alter filamentous growth (Figure S1C), with extension rates (0.3 μm/min; n = 9) identical to that of wild-type cells. These results indicate that the 488-nm pulses had no deleterious effect on filamentous growth and suggest that the perturbation we observe is due to an association of active Cdc42 with its effector. We also examined whether light-dependent recruitment of wild-type Cdc42 (which could be activated by endogenous GEF) altered filamentous growth and approximately 40% of cells (n = 100) displayed altered morphology following photoactivation. Given that upon recruitment of constitutively active Cdc42[G12V]$_{cyto}$ all of the filamentous cells exhibited altered morphology, this activated mutant was used for all subsequent studies.

New Growth Occurs in the Mother Cell or along the Filament

Since growth resumed subsequent to optogenetic recruitment in filamentous cells, we examined where this growth occurs. Strikingly, we observed that new filamentous growth could emerge from either the mother cell or the filament. In the latter case, growth occurred along the filament or resumed at the tip (Figure 2C). New growth, whether in the mother cell or the filament, had an identical extension rate to that of initial growth (Figure 2D), corroborating its physiological relevance. The majority of cells, ~75%, resumed growth at the tip, whereas ~20% of the cells initiated growth in the mother cell and ~5% initiated growth in the filament. Cells with shorter germ tubes (2–6 μm long) were more likely to initiate new growth in the mother cell, whereas cells with longer filaments (8–12 μm long) were more likely to initiate growth in the filament (Figure 2E). Following photo-recruitment, new growth, irrespective of its location, initiated on average 20 min after the last pulse, indicating that it occurred subsequent to the plasma membrane dissociation of Cry2-mCh- Cdc42[G12V]$_{cyto}$. We next examined the location of new growth along the filament as a function of filament length at the time of photoactivation. New growth could occur anywhere along the filament with a preference farther away from the tip with increasing initial filament lengths (Figure 2F). We also examined the angle between the new filament and initial filament when growth occurred in the mother cell. Figure 2G shows that growth occurred predominantly in the distal half of the mother cell (between ± 60° and 180° from the initial filament). Together, these data indicate *de novo* growth site formation and suggest that growth in longer filaments is more refractory to disruption.

Recruitment of Cdc42·GTP Disrupts Endogenous Active Cdc42 Localization

The timing of new filamentous growth relative to light-dependent active Cdc42 recruitment suggested that new growth occurs subsequent to the dissociation of Cry2-mCh-Cdc42[G12V]$_{cyto}$ from the membrane. To determine whether active Cdc42 recruitment either directly induces polarized growth or instead resets cell polarity, we followed the distribution of a reporter for active Cdc42 derived from the *S. cerevisiae* Cdc42 effector protein Gic2 (Cdc42- and Rac-interactive binding [CRIB]-mCh) (Corvest et al., 2013). In filamentous cells, a cluster of active Cdc42 observed at the filament apex prior to photoactivation (Figure 3A; Video S1) was no longer detectable following Cry2-GFP-Cdc42 [G12V]$_{cyto}$ recruitment. Quantitation of the ratio of growth site (tip) plasma membrane to cytoplasmic CRIB-mCh signal revealed an average reduction of ~2-fold following the second or third photoactivation (Figure 3B). Just prior to new growth, ~30 min after the last photoactivation pulse (28 ± 6 min; n = 15 cells), a cluster of active Cdc42 was again observed. Together, these results indicate that recruitment of Cdc42•GTP disrupts the initial cluster of active Cdc42, which subsequently forms a cluster at a distinct location.

Endocytic Sites Disperse Subsequent to Cdc42·GTP Recruitment

As our results suggested that photo-recruitment of active Cdc42 resets cell polarity, we examined whether the sites of endocytosis and exocytosis remained localized. In growing hyphal filaments, endocytic sites localize as a collar 1–3 μm from the filament tip (Caballero-Lima et al., 2013; Ghugtyal et al., 2015;

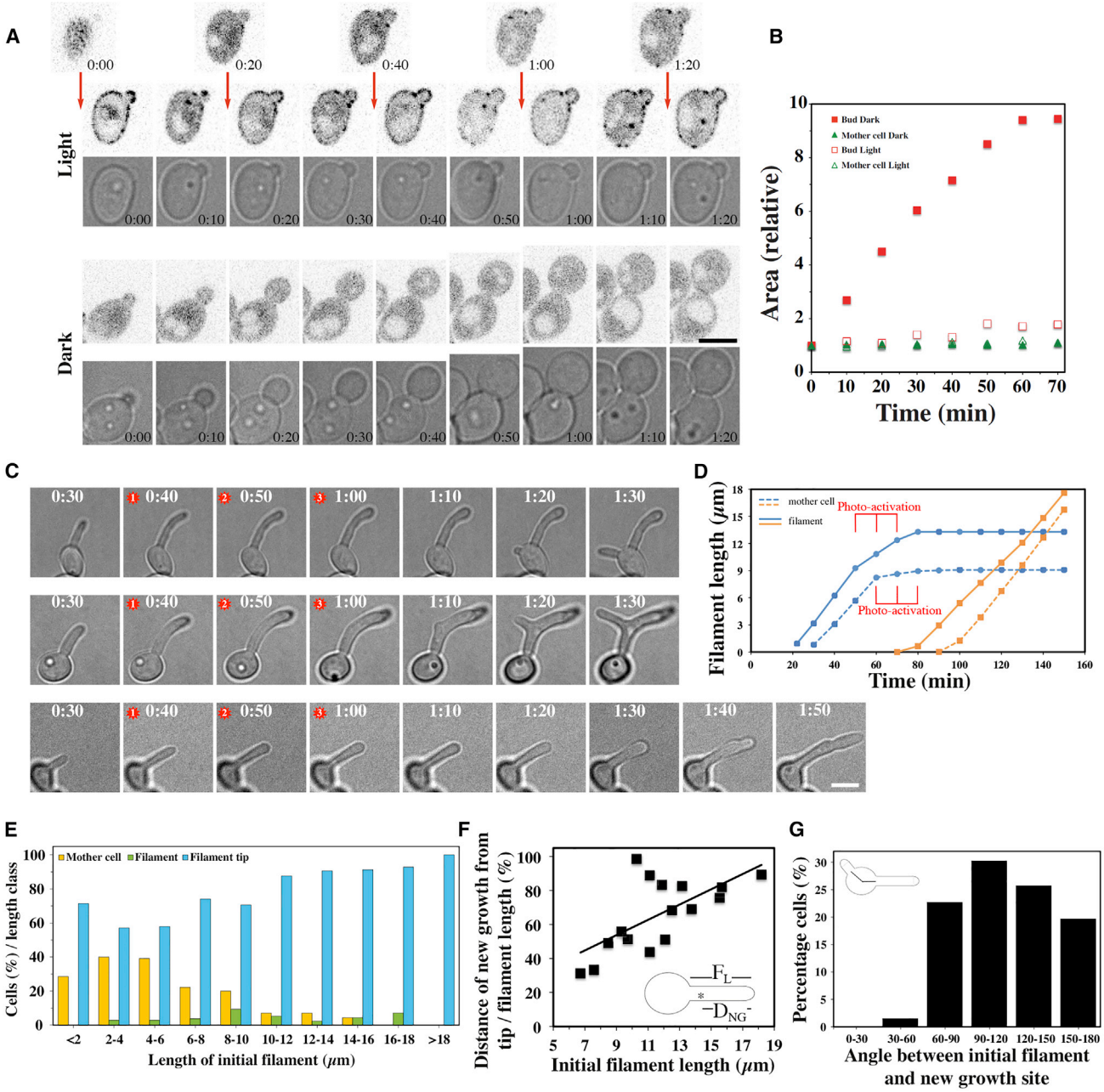

Figure 2. Plasma Membrane Recruitment of Cdc42·GTP Disrupts Polarized Growth

(A) Polarized budding growth is blocked following Cdc42•GTP recruitment. Strain was incubated as in Figure 1B and either exposed (Light) or not (Dark) to 488-nm light, as in Figure 1C. mCh (upper panel) and differential interference contrast (DIC) images (lower panel) for each time course are shown.

(B) Quantification of bud and mother cell area following photo-recruitment of Cdc42•GTP. Average relative area in cells (n = 5) with photoactivation at 0, 20, 40, and 60 min.

(C) Following recruitment of Cdc42•GTP in filamentous cell, new growth can occur in the mother cell or along the filament. Strain as in Figure 1B was incubated on agar pads containing serum at 37°C and exposed to 3 pulses of 488-nm light (red stars). In the absence of 488-nm light, filamentous cells grew normally.

(D) New growth occurs at same rate as the initial filament. Length of new filament emerging either from filament (solid lines) or mother cell (dashed lines) is shown.

(E) New growth location depends on initial filament length. Percentage of cells in each filament length class in which new growth emerged from mother cell (yellow), filament (green), or resumed at tip (blue). Strain and conditions as in Figure 2C. Quantification of 425 cells (from 11 experiments) followed by time-lapse microscopy (n = 15–80/length class).

(F) New growth in filament occurs preferentially farther from the tip for cells with longer initial filaments. Strain and conditions as in Figure 2C. Location of growth in filament divided by initial filament length is shown (n = 16; 8 experiments followed by time-lapse microscopy).

(G) New growth in the mother cell occurs medially to initial filament. Strain and conditions as in Figure 2C. Angle of the new germ tube relative to the initial filament was quantified (n = 66 cells; 9 time-lapse experiments). Scale bar, 5 μm.

Zeng et al., 2012) and secretory vesicles localize to the tip, in a cluster referred to as a Spk (Riquelme, 2013; Riquelme and Sánchez-León, 2014). We visualized sites of endocytosis using actin-binding protein 1 (Abp1), which localizes to this endocytic collar. Following recruitment of active Cdc42 to the plasma membrane, the tip cluster of the Abp1-mCh dispersed, and ~10 min after the last photoactivation pulse, there was an increase in Abp1-mCh signal in the mother cell, which clustered at the incipient germ tube ~30 min later (Figures 3C and 3D; Video S2). These results suggest that endocytosis at the filament tip is disrupted by photo-recruitment of active Cdc42 over the plasma membrane.

Cdc42·GTP Recruitment Results in a *De Novo* Secretory Vesicle Cluster

To visualize secretory vesicles, we examined a number of proteins that associate with these vesicles and have been localized to the Spk. These include the myosin light chain, Mlc1, the Rab GTPases, Sec4 and Ypt31, and the Sec4 GEF, Sec2, which associate on secretory vesicles in *S. cerevisiae* (Ortiz et al., 2002; Wagner et al., 2002), as well as localize to the Spk at the filament tip (Bishop et al., 2010; Crampin et al., 2005; Jones and Sudbery, 2010; Li et al., 2007; Ortiz et al., 2002; Pantazopoulou et al., 2014; Sánchez-León et al., 2015). Strikingly, immediately following plasma membrane recruitment of Cdc42·GTP, a second cluster of Mlc1-mCh was observed, typically in the cell body or base of the filament (Figures 3E and S2; Video S3, compare with Video S4). Note that while one additional cluster of Mlc1 was observed subsequent to photoactivation, occasionally we observed 2 or more clusters. The initial cluster of Mlc1-mCh persisted for some time after the appearance of the second Mlc1 cluster, moved down the filament over time, and eventually appeared to coalesce with the second Mlc1 cluster. This coalesced Mlc1 cluster, which was always localized to the cell cortex, was highly dynamic before settling down to the site of the incipient germ tube (Figures 3F and S2). In all cells examined, the final location of the secretory vesicle cluster at the cell cortex was precisely where the new filament emerged, suggesting that this vesicle cluster is physiologically relevant. While we focused on cells in which plasma membrane recruitment of Cdc42·GTP ultimately resulted in filamentous growth at new location (Figures 3E, 3F, and S2; Video S3), we also examined cells in which, after a pause, tip growth resumed. Figure S3A shows a second cluster of Mlc1-mCh, observed frequently in the cell body, which behaved similarly as that in Figures 3E, 3F, and S2. However, in these cells, this second cluster of Mlc1-mCh did not settle at new location from which a new filament would emerge. When we compared cells with the same initial filaments length, it appeared that more photoactivation pulses were required to disrupt the initial Spk when new growth resumed at the tip (Figures 3E and S2 compared to Figure S3A), suggesting that when the growth site was more robust, new growth resumed at the tip.

Hence, we examined whether there was a correlation between the ability to disrupt the Spk and filament length upon photoactivation. Fewer photoactivation pulses were required to disrupt the initial Spk in cells with shorter filaments than in cells with longer filaments (Figure 3G). These results suggest that the growth site in shorter filaments is less robust compared to that of longer filaments. In the absence of photoactivation, the cluster of Mlc1 was restricted to the tip and moved as the filament extended at a rate of ~0.3 μm/min (Video S4). Following photoactivation, there was a dramatic increase in the instantaneous velocity of the Mlc1 cluster, with peaks of up to 10-fold higher, i.e., 3–4 μm/min (Figure S4A), inconsistent with association and dissociation. The shape of the Mlc1 cluster, which appeared as a sphere (projected onto the XY plane) in the absence of photoactivation, elongated along the axis of movement following photoactivation, further consistent with its displacement (Figure S4B). While photo-recruitment of active Cdc42 blocked polarized growth, tip swelling was observed (Figure 2C), suggesting a switch to isotropic growth. Unstable, dynamic polarity clusters, in particular active Cdc42 visualized by the CRIB domain, have been observed in *S. pombe* upon slowing or stopping cell growth (Bendezú and Martin, 2013; Bonazzi et al., 2014, 2015; Haupt et al., 2018; Mutavchiev et al., 2016), hence we examined whether such dynamic behavior of the Mlc1 cluster was observed upon decreasing growth rate using an *arl1* mutant that has a decreased filament extension rate, as well as frequently abandoning tip growth (Labbaoui et al., 2017). In these mutant cells, the Spk was unaffected by the reduced growth rate, and upon abandoning growth at the filament tip, a new vesicle cluster only became visible at the incipient germ tube site either concomitant with or subsequent to the loss of the initial cluster (Figure S3B). Together these results indicate that recruitment of active Cdc42 over the plasma membrane results in a *de novo* cluster of Mlc1, which is highly dynamic and not a consequence of reduced growth rate.

In *C. albicans* hyphae, while Mlc1 is observed at the Spk with little to no signal elsewhere in the cell (Crampin et al., 2005; Jones and Sudbery, 2010), Sec4 is found both at this apical location and associated with individual secretory vesicles (Ghugtyal et al., 2015; Jones and Sudbery, 2010; Li et al., 2007; Wakade et al., 2017). Using mScarlet (mSc) fused to Sec4, we followed the distribution of secretory vesicles after photoactivation. Figure 4A (Video S5 compared to Video S4 without photoactivation) shows Sec4 at the tip of an emerging germ tube and, within 1 min of photo-recruitment of active Cdc42, a new cluster of Sec4 forms in the mother cell. This new cluster was highly dynamic (Figure S4C), similar to the dynamics of the Mlc1 cluster, and in a strain expressing both mSc-Sec4 and Mlc1-miRFP, these two proteins co-localized throughout the time course (Figure S4D; Video S6). To provide additional evidence that this new cluster of Mlc1 and Sec4 was composed of secretory vesicles, we examined two additional secretory vesicle components, the Sec4 GEF, Sec2, and the Rab11 homolog, Ypt31; the former is found at the Spk in *C. albicans* (Bishop et al., 2010), and the latter localized to secretory vesicles in *S. cerevisiae*, *N. crassa*, and *A. nidulans* and the Spk in *N. crassa*, *A. nidulans*, and *C. albicans* (Ortiz et al., 2002; Pantazopoulou et al., 2014; Sánchez-León et al., 2015; Wakade, 2017). Immediately following plasma membrane photo-recruitment of active Cdc42, we observed that Sec2 and Ypt31 co-localized with Mlc1 at the new cluster (Figures 4B, 4C, S5A, and S5B), despite the relatively low signals of Sec2-mSc and Ypt31-mCh. To determine whether this new cluster of secretory vesicles also contained markers for other membrane compartments, we used

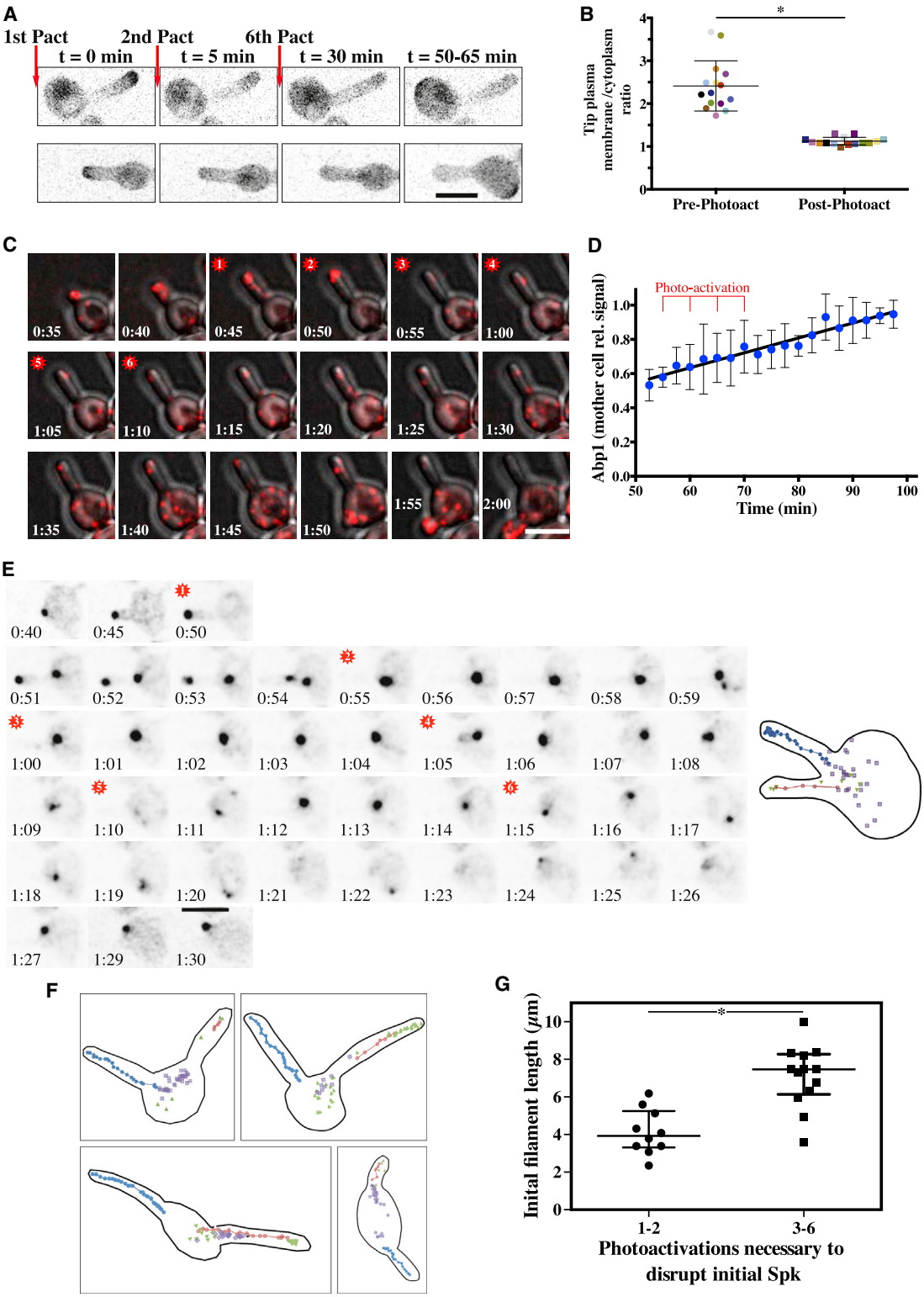

Figure 3. Photo-Recruitment of Cdc42·GTP Disrupts Endogenous Cdc42 Activation and Endocytosis Sites at Filament Tip

(A) Following photoactivation, active Cdc42 at the filament tip is no longer detectable. A strain expressing CibN-Ct_{Rac1}, Cry2-GFP-Cdc42[G12V]$_{cyto}$, and CRIB-mCh was incubated as in Figure 2C and exposed to 6 pulses of 488-nm light every 5 min. DIC and maximum projection mCh images are shown from

(legend continued on next page)

strains expressing Mlc1-miRFP and either the endoplasmic reticulum (ER) marker phosphatidylinositol-4-phosphate phosphatase, Sac1 (Foti et al., 2001; Weiner et al., 2019), or the late Golgi maker Arf GEF, Sec7 (Ghugtyal et al., 2015). Figures 4D and S5C show that the ER is distinct from the new cluster labeled with Mlc1, which is best visualized in a three-dimensional reconstruction (Video S7), indicating there is a gap between the ER membranes and the Mlc1 cluster. In *C. albicans* hyphae, the Golgi cisternae are somewhat enriched at the apex (Ghugtyal et al., 2015; Rida et al., 2006), and consistently, prior to plasma membrane photo-recruitment of active Cdc42, Sec7-mSc labeled Golgi cisternae also clustered behind the Spk (Figures 4E and S5D). Recruitment of active Cdc42 resulted in dispersal of the Golgi cisternae, which appeared to transiently align between the two vesicle clusters without any detectable overlap (Figures 4E and S5D). Together, these data indicate that photo-recruitment of active Cdc42 results in a *de novo* secretory vesicle cluster, which is distinct from ER and Golgi membrane compartments.

We noted that the new cluster of vesicles, visualized with mSc-Sec4, appeared larger than the initial cluster (Figure 4A; Video S5). Quantitation of its maximal cross-sectional area revealed a 4.7-fold increase (n = 14; compared to the initial cluster), and the average signal of this new cluster increased ~4-fold, following photoactivation, concomitant with a decrease in the cytoplasmic signal (Figure S4E). Furthermore, the ratio of Sec4 to Mlc1 signal in a strain co-expressing mSc-Sec4 and Mlc1-miRFP increased 3- to 4-fold, resulting in a shift in the cluster of vesicles from magenta (Mlc1) to green (Sec4) upon photoactivation and then back to magenta ~10 min after the last photoactivation pulse (Figures S4D, S4F, and S4G; Video S6). Sec4 recruitment was observed at both the initial Spk and the new dynamic vesicle cluster (Figure S4H). Unfortunately, the relatively low signals of Ypt31-mCh and Sec2-mSc prevented such extensive analyses, yet immediately following photoactivation, we observed at the new vesicle cluster a similar increase of Ypt31 (2- to 3-fold, n = 13, compared to Mlc1-miRFP levels) and in two-thirds of the cells quantified (n = 12) a transient increase of Sec2 (~2-fold compared to Mlc1-miRFP levels). Together, these data suggest that photo-recruitment of active Cdc42 results in a *de novo* secretory vesicle cluster, with a concomitant increase level of Sec4 and Ypt31.

Cdc42·GTP Recruitment Disrupts Sec3 Localization and Reduces Turnover of Secretory Vesicles

As the new cluster of secretory vesicles was substantially larger than the initial Spk and hyphal filaments did not appear to extend (polarized tip growth) following photo-recruitment of active Cdc42, we speculated that there was a defect in polarized secretion. Since the exocyst subunit Sec3, which localizes to the cortical tip of the hyphae in *C. albicans* (Ghugtyal et al., 2015; Jones and Sudbery, 2010; Li et al., 2007), is critical for targeting and/or tethering secretory vesicles (Luo et al., 2014) and binds active Cdc42 (Zhang et al., 2001) in *S. cerevisiae*, we examined whether it remains at the filament tip subsequent to photo-recruitment of active Cdc42. Figures 5A and 5B show that upon photo-recruitment of active Cdc42, Sec3-mSc signal is no longer detectable at the apex, which we expect would lead to a reduction in polarized vesicle fusion with the plasma membrane. Therefore, one expects that the turnover of secretory vesicles in this new cluster should be reduced, compared to that of the initial Spk. The dynamics of secretory vesicle turnover was determined using fluorescence recovery after photobleaching (FRAP) (Figure 6A). The FRAP $t_{1/2}$ of the initial Spk, 8.1 ± 2.7 s (n = 10), was in good agreement with the value determined previously (7.3 s) (Jones and Sudbery, 2010), while the new cluster of secretory vesicles was significantly less dynamic with a FRAP $t_{1/2}$ of 22.0 ± 9.0 s (n = 11) (Figure 6B), consistent with a reduction in vesicle fusion with plasma membrane.

The Actin Cytoskeleton Is Associated with the New Vesicle Cluster

The delivery of secretory vesicles to the Spk requires actin cables, which emanate from this structure; indeed, depolymerization of F-actin disrupts the Spk (Crampin et al., 2005). To determine whether actin cables were intact following active Cdc42 photo-recruitment, actin was visualized in fixed cells expressing Mlc1-miRFP after the appearance of two clusters (Figure 7A). Figure 7A (Light) shows an apparent decrease in the actin cables around the initial Spk following photoactivation, while the new cluster appears to have actin cables emanating from it, frequently oriented toward the back of the mother cell. This raises the attractive possibility that movement of this new cluster might be actin driven, much like actin-dependent propulsion of endosomes, pinosomes, and phagosomes

2 time-lapses. Photo-recruitment did not result in an increase in the CRIB-mCh reporter on the plasma membrane, suggesting that the Cry2 fusion does not efficiently bind the reporter, perhaps due to the Cry2-GFP moiety.

(B) The level of active Cdc42 at the growth site decreases following photoactivation. The ratio of tip to cytoplasmic signal was determined at the 1st and either 2nd or 3rd photoactivation as in Figure 3A (n = 15 cells; 5 experiments); colors indicate same cell. The average and SD are shown, and the difference was statistically significant using an unpaired t test, $p < 0.0001$.

(C) Endocytosis sites become dispersed upon photo-recruitment of Cdc42•GTP. A strain expressing CibN-Ct_{Rac1}, Cry2-GFP-Cdc42[G12V]$_{cyto}$, and Abp1-mCh was incubated as in Figure 3A (red stars, photo-activations). DIC and maximum projection mCh images are shown from a representative time-lapse.

(D) Abp1 in the mother cell increases following photoactivation. Quantification of Abp1-mCh signal in the mother cell (n = 7; 3 experiments) over time is shown, with the signal at time of new germ tube emergence set to 1. The average and SD are shown.

(E) Cluster of secretory vesicles becomes highly dynamic following recruitment of active Cdc42. A strain expressing CibN-Ct_{Rac1}, Cry2-GFP-Cdc42[G12V]$_{cyto}$ and Mlc1-mCh was incubated as in Figure 3A. DIC and sum projection mCh images are shown from a representative time-lapse (images every 2.5 min prior to photoactivation and 1 min, thereafter, left panel). Right panel shows location of Mlc1 cluster in the final cell shape with location in initial extending germ tube (red), existence of two clusters (green), dynamic cluster in mother cell (purple), and cluster in final extending germ tube (blue).

(F) Mlc1 cluster is highly dynamic following recruitment of active Cdc42. Location of Mlc1 cluster in 4 cells as in Figure 3E.

(G) Mlc1 cluster is more easily disrupted in shorter filaments. Strain as in Figure 3E was analyzed as above and the number of photoactivation pulses necessary to disrupt initial Mlc1 cluster was determined as a function of filament length (n = 25; 9 experiments), followed by time-lapse microscopy. The average and SD are shown, and the difference between cells with shorter and longer filaments was statistically significant using an unpaired t test, $p < 0.0001$. Scale bar, 5 μm.

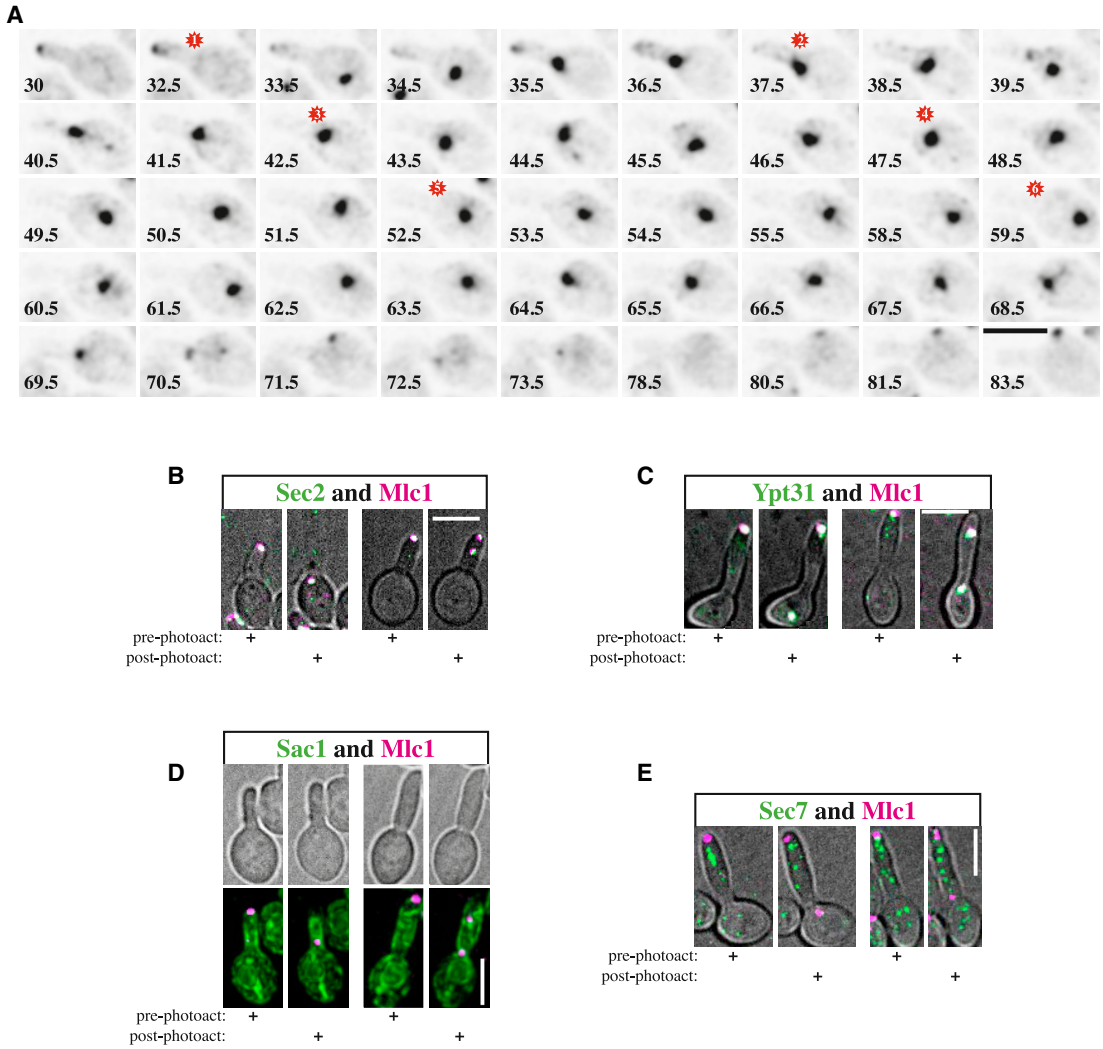

Figure 4. Recruitment of Cdc42·GTP Induces *De Novo* Secretory Vesicle Clustering

(A) Sec4 dynamics following photo-recruitment of active Cdc42. Strain expressing CibN-Ct_{Rac1}, Cry2-GFP-Cdc42[G12V]$_{cyto}$, and mSc-Sec4 was incubated and analyzed as in Figure 3E, and a representative time-lapse is shown.

(B) Sec2 is localized to the new vesicle cluster. A strain expressing CibN-Ct_{Rac1}, Cry2-GFP-Cdc42[G12V]$_{cyto}$, Sec2-3x-mSc, and Mlc1-miRFP was incubated as in Figure 3E, and maximum projections of RFP (green) and miRFP (magenta) images merged with DIC images from a representative time-lapse are shown. Pre-photoactivation denotes < 1 s after 488-nm light exposure and post-photoactivation 2.5 min later.

(C) Ypt31 is localized to the new vesicle cluster. A strain expressing CibN-Ct_{Rac1}, Cry2-GFP-Cdc42[G12V]$_{cyto}$, mCh-Ypt31, and Mlc1-miRFP was incubated and analyzed as described in Figure 4B.

(D) The new vesicle cluster does not overlap with the endoplasmic reticulum. A strain expressing CibN-Ct_{Rac1}, Cry2-GFP-Cdc42[G12V]$_{cyto}$, Sac1-mSc, and Mlc1-miRFP was incubated and analyzed as described in Figure 4B, except pre-photoactivation indicates 1 min prior exposure to 488-nm light and post-photoactivation 5 min later.

(E) The new vesicle cluster is distinct from the late Golgi. A strain expressing CibN-Ct_{Rac1}, Cry2-GFP-Cdc42[G12V]$_{cyto}$, Sec7-3x-mSc, and Mlc1-miRFP was incubated and analyzed as described in Figure 4B. Scale bar, 5 μm.

(Merrifield et al., 1999; Southwick et al., 2003; Taunton et al., 2000).

Modeling Secretory Vesicle Cluster Dynamics

To determine whether this cluster of vesicles moves in a random or directed fashion, we analyzed its movement on the cortex (approximating the mother cell as a sphere) from 10 cells following photoactivation (Figure 7B). First, we derived the colatitude of the cluster with respect to the initial position (θ in Figure S6A), and the square angular displacement (colatitude θ^2) does not depend on time, inconsistent with a pure diffusion process (Figure S6B compared to Figure S6C; Figure S6D). Figure 7C (compared to Figure S7A) confirms that the dynamics of the vesicle cluster is not simply diffusive but rather that movement is strikingly confined to a small region; from the north pole this would be roughly up to the 30th parallel north. These

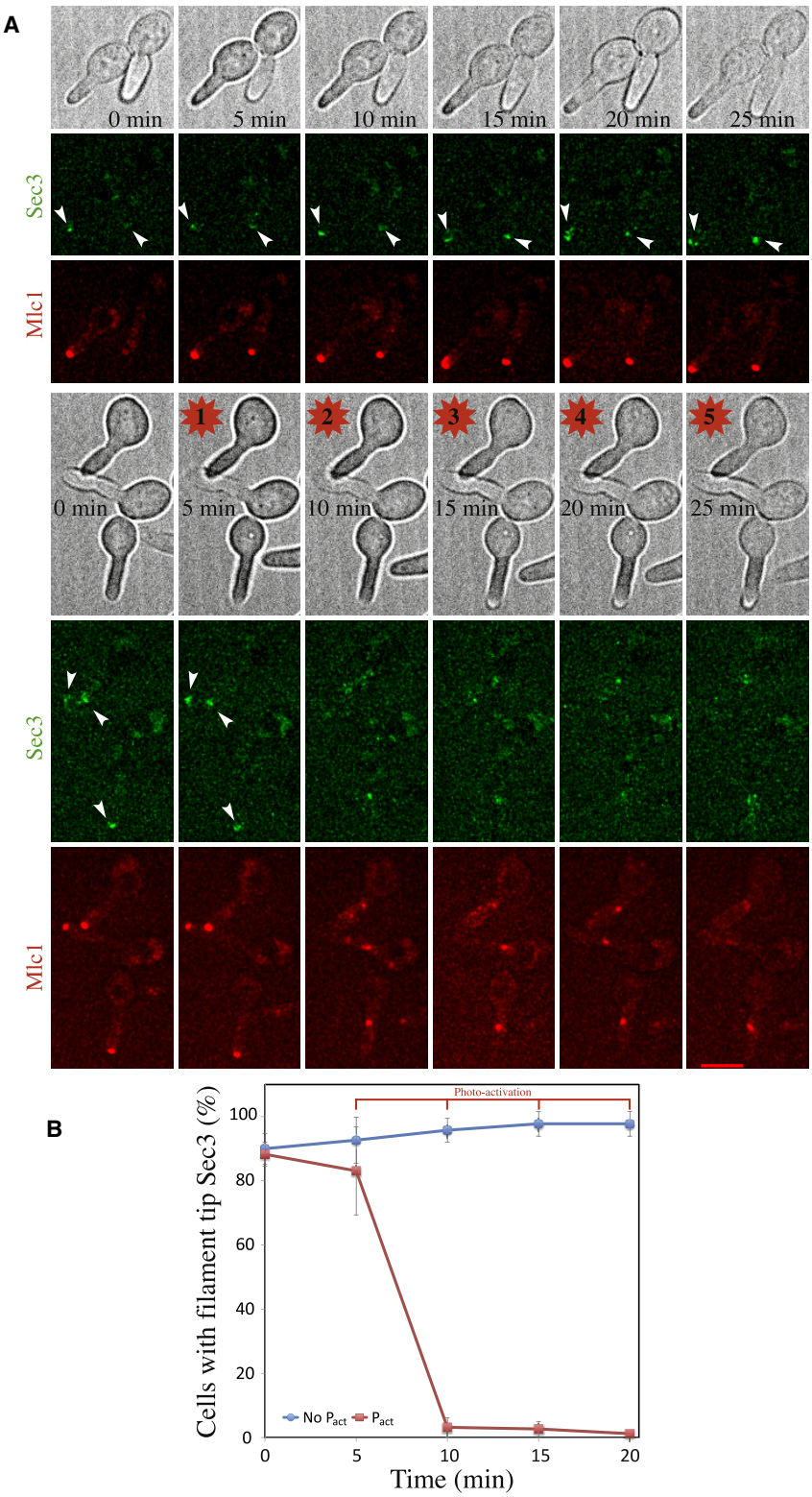

Figure 5. Optogenetic Recruitment of Cdc42·GTP Disrupts Sec3 Filament Tip Localization

(A) Following recruitment of Cdc42·GTP, Sec3 is no longer observed at filament tip. A strain expressing CibN-Ct_{Rac1}, Cry2-GFP-Cdc42[G12V]$_{cyto}$, Sec3-3x-mSc, and Mlc1-miRFP was incubated as in Figure 3E, and maximum projections of RFP (green) and miRFP (red) images are shown from a representative time-lapse (arrowheads indicate Sec3 at tip cortex).

(B) Quantitation of the percentage of cells with Sec3 localized to the hyphal apex upon optogenetic recruitment of Cdc42·GTP. The percentage of cells in which both Sec3-mSc and Mlc1-miRFP were visible at filament tip was quantitated from time-lapses as described above. Cells were exposed or not to 488-nm light (n = 15–30 cells per experiment; 3 experiments) with the mean and standard deviation shown. Scale bar, 5 μm.

conclusions are robust, even for analyses of the early (t < 10 min) or late (t > 15 min) times, corroborating that this effect is not due to a transient in time (compare Figures S7B and S7C). The cluster often moves in a series of short hops, but it occasionally undergoes large jumps (Figure 7C, inset). These long-range displacements, akin to flipping of the poles, were observed in the majority of cells and are also likely to be movement, as intermediate steps were occasionally detected (Figure 7B). We hypothesize that two non-mutually exclusive mechanisms could underlie such vesicle cluster dynamics: (1) actin cytoskeleton confines or drives movement and (2) interactions with the cortex, e.g., a protein anchor or specific lipid environment limits movement (Figure 7D). Disruption of such confining or limiting processes could result in long-range displacements across the cell.

DISCUSSION

We used optogenetic manipulation of cell polarity to reset growth in asymmetric filamentous *C. albicans* cells. A transient increase of the overall level of Cdc42·GTP on the plasma membrane disrupted the cluster of endogenous active Cdc42, the key exocyst subunit Sec3 at the filament tip, and the collar of endocytosis sites proximal to the filament apex. In contrast, a striking *de novo* cluster of secretory vesicles formed, distinct from the ER and Golgi, which had a number of hallmarks of the Spk. Furthermore, it was highly dynamic, moving in an active fashion by hops and jumps, until a new growth site was subsequently established.

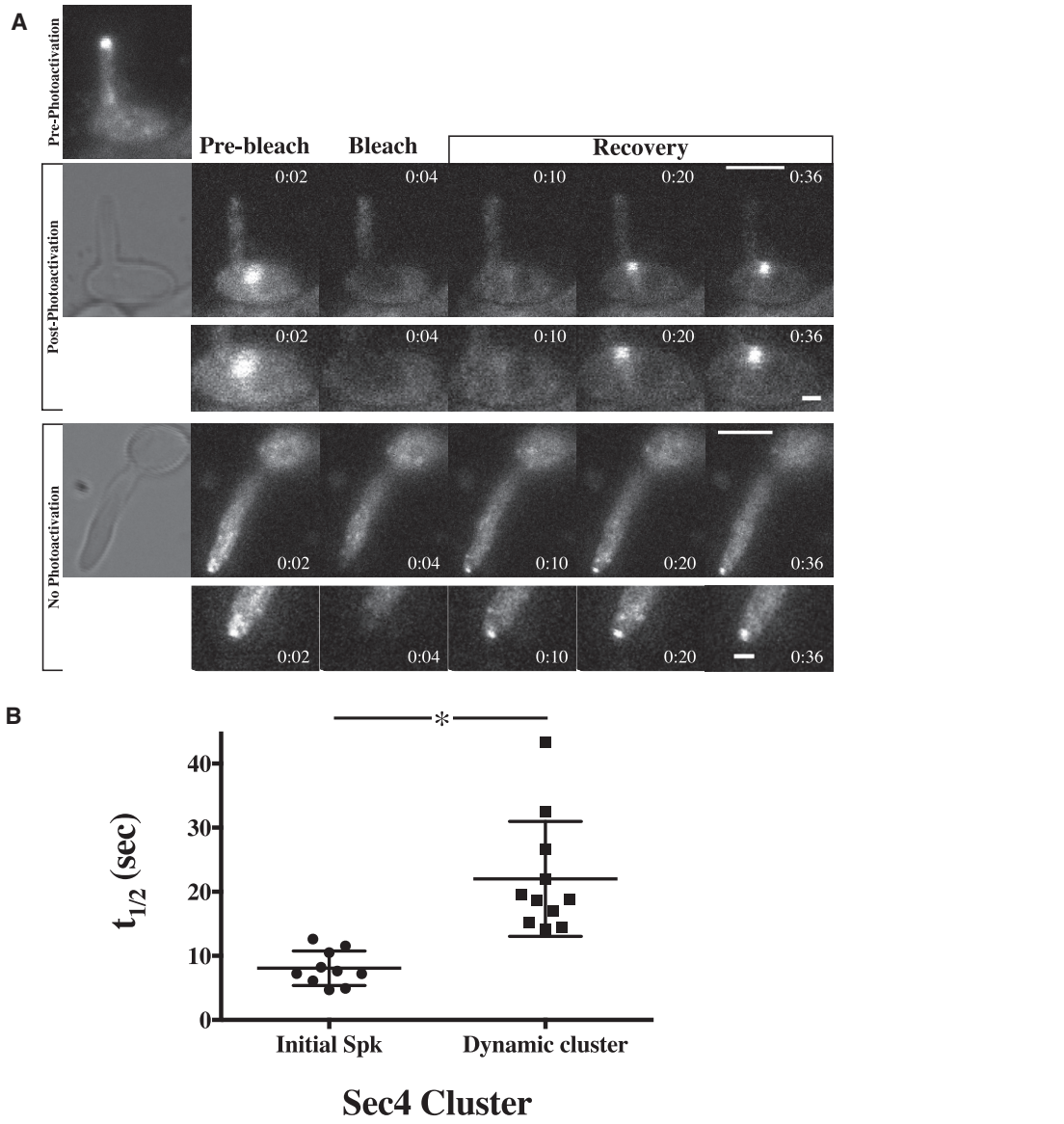

Figure 6. Sec4 Exchanges More Slowly in the New Secretory Vesicle Cluster Than in the Initial Spitzenkörper

(A) Fluorescent recovery after photobleaching of Sec4 prior to or following photo-recruitment of active Cdc42. A strain expressing CibN-Ct_{Rac1}, Cry2-GFP-Cdc42 $[G12V]_{cyto}$, and mSc-Sec4 was incubated as in Figure 4A, RFP images were acquired at indicated times (in seconds), and a representative FRAP experiment is shown. Photobleaching was at 4 s, and a zoom of the region analyzed is shown below. Scale bar, 5 μm and 1 μm in zoom of region.

(B) The half-time for recovery of Sec4 fluorescence is significantly slower in the new cluster. The $t_{1/2}$ for fluorescence recovery was determined for 10–11 cells, with the average and SD shown, and the difference was statistically significant using an unpaired t test, p = 0.0001.

How does this growth reset compare to filament branching? During hyphal growth, branching is critical for increasing biomass and effectively accessing nutrients and occurs laterally, i.e., along the filament, and at the apex (Harris, 2019). During apical branching in *N. crassa*, the extension of the initial apex was substantially reduced and the Spk no longer detectable, whereas they were largely unaffected during lateral branching (Reynaga-Peña et al., 1997; Riquelme and Bartnicki-Garcia, 2004). Also, during apical branching in this fungus, as well as in *Aspergillus niger* and a range of other fungi, a new Spk, visualized by phase contrast imaging, appeared to form *de novo* via a coalescing of vesicles, where a new branch will form (Bartnicki-Garcia et al., 1995; López-Franco and Bracker, 1996; López-Franco et al., 1995; Reynaga-Peña et al., 1997; Riquelme and Bartnicki-Garcia, 2004). Transient retraction of the *N. crassa* Spk from the hyphal apex, coinciding with a reduction in filament extension and an alteration in morphology, has been visualized by following cell wall biosynthetic enzymes, the scaffold protein Spa2, and the membrane dye FM4-64; after retraction, the Spk did not return to the initial apical position, but rather

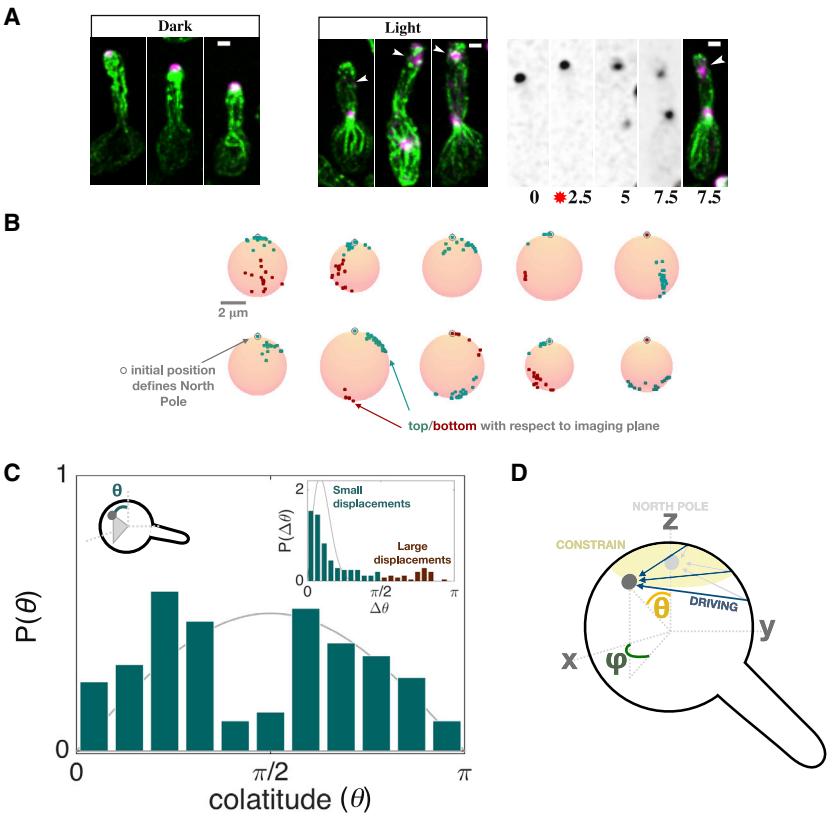

Figure 7. The Actin Cytoskeleton Is Associated with the New Vesicle Cluster, Whose Movement Is Constrained to a Small Region

(A) Actin cables emanate from newly formed cluster of secretory vesicles. A strain expressing CibN-Ct_{Rac1}, Cry2-GFP-Cdc42[G12V]$_{cyto}$, and Mlc1-miRFP was incubated and exposed to 488-nm light (Light) or not (Dark). After photoactivation (5 min), cells were fixed and the actin cytoskeleton visualized. In the right panel, cells were imaged every 2.5 min prior to fixing (7.5 min). Maximum projections of fixed cells with F-actin (green) and Mlc1 (magenta) shown. Scale bar, 1 μm.

(B) Positions of the experimentally determined vesicle clusters on mother cell cortex. The mother cell shape was approximated as a sphere and the x-y co-ordinates of the cluster were projected on the surface. The north pole coincides with the first cluster position in 10 cells expressing Mlc1-mCh, with spots indicating the top (green) and bottom (red) hemisphere relative to the central focal plane, respectively.

(C) Probability distribution of the cluster's colatitude for all cells at all times confirms that motion of the cluster is strikingly different from a purely diffusive process (line is theoretical prediction for diffusion at long times, no integral in time), $p = 3 \times 10^{-7}$; Kolmogorov-Smirnov test. Bimodality indicates that the cluster mostly populates a region proximal to the initial point, in addition to a distal region. The probability distribution of angular displacement in a single time step (inset) demonstrates that the cluster occasionally undergoes large jumps in a single step (dark red, frequency 18%), while most of the time it proceeds in smaller hops (green, frequency 82%). The line is the best fit of the theoretical prediction for pure diffusion to the data, inconsistent with the data ($p = 5 \times 10^{-13}$; Kolmogorov-Smirnov test). From this fit to the theoretical prediction, we obtained $\tau = 0.07$ ($t = 1$ min acquisition time and $R = 2.7$ μm is the average mother cell radius), hence this τ value corresponds to $D = 0.26$ μm^2/min.

(D) Schematic of the constrained movement of vesicle cluster. The three coordinates that define cluster location are the angles θ and φ and radius r. The region of restricted vesicle movement is highlighted in yellow, with initial cluster location indicated in light gray and subsequent location in dark gray. Light gray (initial) and dark blue (subsequent) arrows indicate the contribution of forces driving movement, e.g., actin cable polymerization.

an additional Spk appeared to form at the apex (Araujo-Palomares et al., 2009; Sánchez-León et al., 2011; Verdín et al., 2009). Although we did not observe new growth emerge within several microns of the hyphal apex, the extension of the initial tip was dramatically reduced upon photo-recruitment of active Cdc42 in *C. albicans*, suggesting that this process is similar, in some respects, to apical branching in filamentous fungi. However, it should be noted that extension rates are 10- to 100-fold slower in *C. albicans* compared to these fungi, whose growth also depends on microtubule cytoskeleton, and that the Spk composition is different (Weiner et al., 2019).

What is the relationship between growth and the *de novo* vesicle cluster? In *S. cerevisiae* and *S. pombe*, recent studies in symmetrical cells, such as spores or sexually differentiated cells exposed to low mating pheromone concentrations, have revealed situations in which polarity clusters can switch from stable behavior at a growth site to unstable wandering around the cell cortex or vice versa (Bendezú and Martin, 2013; Bonazzi et al., 2015; Bonazzi et al., 2014; Dyer et al., 2013; Haupt et al., 2018; Mutavchiev et al., 2016). These unstable polarity clusters were associated with a slowing or stopping of cell growth. Examination of a *C. albicans* mutant decreased in filament extension and altered in restricting growth to a single site (Labbaoui et al., 2017) also exhibited an unstable, wandering cluster of active Cdc42, yet in this mutant we observed only one cluster of secretory vesicles at a time, without dynamic behavior, visible at the new incipient germ tube site when the initial Spk was essentially undetectable (Figure S3B). In the recent study of Haupt et al. (2018), *S. pombe* growth inhibition by osmotic shock and physical confinement resulted in perturbation of the actin distribution. Blocking growth in *C. albicans* hyphae by actin depolymerization or in a *sec3* exocyst mutant disrupted the Spk vesicle cluster (Crampin et al., 2005; Jones and Sudbery, 2010; Li et al., 2007; Weiner et al., 2019). In contrast, in the present study, photo-recruitment of active Cdc42 did not alter actin patches and cables during the initial 5 min (Figures 3C and 7A), in which a new cluster of vesicles was already observed (Figures 3E and 4A). Hence, the cluster of secretory vesicles observed in this study appears to be distinct from the polarity cluster visualized with the CRIB reporter in the *S. pombe* study (Haupt et al., 2018), in which secretory vesicle components including a type V myosin, a cargo glucan synthase, and a v-SNARE were also less polarized at the cell tips upon blocking growth. Altogether, the distribution and dynamics of the vesicle cluster that forms

upon photo-recruitment of active Cdc42 does not appear to be solely due to blocking growth and transient destabilization of polarity. However, we consider it likely that feedback between the polarity site and the vesicle cluster via actin-cable-dependent transport, as reported in *S. pombe* (Bonazzi et al., 2015), is also implicated in the dynamics of this cluster in *C. albicans*.

What mechanisms underlie vesicle cluster dynamics? The cluster of vesicles formed immediately after photo-recruitment of active Cdc42 appears to have similarities to the initial Spk. First, this new cluster had actin cables emanating from it like the Spk, except that the cables cluster essentially on the distal side of the Spk. Second, four different proteins that localize to the Spk—a myosin light chain, two Rab GTPases, and a Rab GEF—were also found at this new vesicle cluster. In contrast, the new cluster of vesicles was not restricted to the filament apex, was highly dynamic, and the turnover of secretory vesicles was reduced compared to the Spk. Further knowledge of the Spk composition will be important for more in-depth comparison of these two structures. Our data indicate that the new cluster of vesicles undergoes active, directed movement. We envision two related driving forces for the movement of the new cluster of vesicles: (1) actin polymerization driven propulsion, similar to that observed with different organelles (Merrifield et al., 1999; Southwick et al., 2003; Taunton et al., 2000), and (2) actin-dependent myosin motors. In both of these scenarios, an intact actin cytoskeleton would be crucial, as it is for Spk integrity (Crampin et al., 2005; Jones and Sudbery, 2010; Weiner et al., 2019). Specifically, actin cables are critical in both cases, either to generate force upon elongation, when anchored at the cell cortex, or to function as tracks along which vesicle-associated motors move. We favor the former possibility, as it is hard to envision sufficient coordination of a large number of vesicle-associated motors—net displacement would be dramatically reduced as a function of number of motors. It will be necessary to correlate the displacement of the vesicle cluster with a precise number of actin cables and their length and curvature in order to distinguish between these possibilities.

In *N. crassa* and *A. gossypii*, the presence of a Spk correlated with hyphal extension rate, suggesting that this structure is a buildup of vesicles due to limiting fusion with the plasma membrane at the apical growth site (Araujo-Palomares et al., 2007; Köhli et al., 2008). Our results indicate that even in the absence of apical filament extension, a cluster of vesicles formed that appeared similar to the Spk, suggesting that clustering of secretory vesicles does not require directional growth. Our FRAP results suggest that exchange of secretory vesicles into and out of this new cluster was somewhat slower than that of the Spk. We propose that photo-recruitment of active Cdc42 resets growth by disrupting a site-specific link to the initial cluster of vesicles, which is likely to be the exocyst subunit Sec3; concomitantly, a vesicle cluster is generated elsewhere in the cell. This highly dynamic new cluster moves in a confined area with occasional large displacements, and modeling indicates that this behavior is likely to be a constrained or driven active process. In this scenario, re-establishment of a cap of endogenous active Cdc42 at a new location would anchor the cluster of secretory vesicles, facilitating subsequent fusion with the plasma membrane. Our results reveal that secretory vesicle clustering can occur in the absence of directional growth in an asymmetric cell, suggesting that such vesicle clusters found in fungi, plants, and neurons could precede stabilization of a growth site.

STAR★METHODS

Detailed methods are provided in the online version of this paper and include the following:

- KEY RESOURCES TABLE
- LEAD CONTACT AND MATERIALS AVAILABILITY
- EXPERIMENTAL MODEL AND SUBJECT DETAILS
  - Strains
- METHOD DETAILS
  - Strain and plasmid construction
  - Microscopy
  - Modeling
- QUANTIFICATION AND STATISTICAL ANALYSIS
- DATA AND CODE AVAILABILITY

SUPPLEMENTAL INFORMATION

Supplemental Information can be found online at https://doi.org/10.1016/j.celrep.2019.07.062.

ACKNOWLEDGMENTS

We thank J. Konopka and Y. Wang for reagents; S. Bogliolo, H. Labbaoui, M. Mondin, S. Schaub, and S. Lachambre for assistance; R. Wakade for the pEXPARG-YPT31p-mCh-Ypt31 construct; and F. Besse and P. Follette for comments on the manuscript. This work was supported by the CNRS, INSERM, UCA, and ANR (UCA JEDI, ANR-15-IDEX-01; SIGNALIFE, ANR-11-LABX-0028-01; FORFUNIGO, ANR-16-CE13-0010-01; DYNCELLPOL, ANR-19-CE13), CNRS PICS 2FORECAST, FRM (to P.M.S.), and EU FP7 as well as H2020 grants (PITN-GA-2013-607963 and MSCA-ITN- 2015-675407) and the Platform of Resources in Imaging and Scientific Microscopy (PRISM) facility.

AUTHOR CONTRIBUTIONS

Conceptualization, R.A.A. and M.B.; Methodology, P.M.S., C.P., A.S., and R.A.A.; Software, A.S.; Formal Analysis, A.S.; Investigation, P.M.S. and R.A.A.; Writing – Original Draft, R.A.A.; Writing – Review & Editing, M.B. and R.A.A.; Project Administration, R.A.A.; Funding Acquisition, M.B. and R.A.A.; Supervision, M.B. and R.A.A.; Visualization, R.A.A. and A.S.

DECLARATION OF INTERESTS

The authors declare no competing interests.

Received: December 30, 2018
Revised: April 22, 2019
Accepted: July 18, 2019
Published: August 20, 2019

REFERENCES

Araujo-Palomares, C.L., Castro-Longoria, E., and Riquelme, M. (2007). Ontogeny of the Spitzenkörper in germlings of *Neurospora crassa*. Fungal Genet. Biol. *44*, 492–503.

Araujo-Palomares, C.L., Riquelme, M., and Castro-Longoria, E. (2009). The polarisome component SPA-2 localizes at the apex of *Neurospora crassa* and partially colocalizes with the Spitzenkörper. Fungal Genet. Biol. *46*, 551–563.

Araujo-Palomares, C.L., Richthammer, C., Seiler, S., and Castro-Longoria, E. (2011). Functional characterization and cellular dynamics of the CDC-42 - RAC - CDC-24 module in *Neurospora crassa*. PLoS ONE *6*, e27148.

Bartnicki-Garcia, S., Bartnicki, D.D., Gierz, G., López-Franco, R., and Bracker, C.E. (1995). Evidence that Spitzenkörper behavior determines the shape of a fungal hypha: a test of the hyphoid model. Exp. Mycol. *19*, 153–159.

Bassilana, M., Blyth, J., and Arkowitz, R.A. (2003). Cdc24, the GDP-GTP exchange factor for Cdc42, is required for invasive hyphal growth of *Candida albicans*. Eukaryot. Cell *2*, 9–18.

Bassilana, M., Hopkins, J., and Arkowitz, R.A. (2005). Regulation of the Cdc42/Cdc24 GTPase module during *Candida albicans* hyphal growth. Eukaryot. Cell *4*, 588–603.

Bendezú, F.O., and Martin, S.G. (2011). Actin cables and the exocyst form two independent morphogenesis pathways in the fission yeast. Mol. Biol. Cell *22*, 44–53.

Bendezú, F.O., and Martin, S.G. (2013). Cdc42 explores the cell periphery for mate selection in fission yeast. Curr. Biol. *23*, 42–47.

Bendezú, F.O., Vincenzetti, V., Vavylonis, D., Wyss, R., Vogel, H., and Martin, S.G. (2015). Spontaneous Cdc42 polarization independent of GDI-mediated extraction and actin-based trafficking. PLoS Biol. *13*, e1002097.

Bernardo, S.M., Rane, H.S., Chavez-Dozal, A., and Lee, S.A. (2014). Secretion and filamentation are mediated by the *Candida albicans* t-SNAREs Sso2p and Sec9p. FEMS Yeast Res. *14*, 762–775.

Bibeau, J.P., Kingsley, J.L., Furt, F., Tüzel, E., and Vidali, L. (2018). F-Actin Mediated Focusing of Vesicles at the Cell Tip Is Essential for Polarized Growth. Plant Physiol. *176*, 352–363.

Bishop, A., Lane, R., Beniston, R., Chapa-y-Lazo, B., Smythe, C., and Sudbery, P. (2010). Hyphal growth in *Candida albicans* requires the phosphorylation of Sec2 by the Cdc28-Ccn1/Hgc1 kinase. EMBO J. *29*, 2930–2942.

Bonazzi, D., Julien, J.D., Romao, M., Seddiki, R., Piel, M., Boudaoud, A., and Minc, N. (2014). Symmetry breaking in spore germination relies on an interplay between polar cap stability and spore wall mechanics. Dev. Cell *28*, 534–546.

Bonazzi, D., Haupt, A., Tanimoto, H., Delacour, D., Salort, D., and Minc, N. (2015). Actin-Based Transport Adapts Polarity Domain Size to Local Cellular Curvature. Curr. Biol. *25*, 2677–2683.

Bou Daher, F., and Geitmann, A. (2011). Actin is involved in pollen tube tropism through redefining the spatial targeting of secretory vesicles. Traffic *12*, 1537–1551.

Bove, J., Vaillancourt, B., Kroeger, J., Hepler, P.K., Wiseman, P.W., and Geitmann, A. (2008). Magnitude and direction of vesicle dynamics in growing pollen tubes using spatiotemporal image correlation spectroscopy and fluorescence recovery after photobleaching. Plant Physiol. *147*, 1646–1658.

Brand, A.C., Morrison, E., Milne, S., Gonia, S., Gale, C.A., and Gow, N.A. (2014). Cdc42 GTPase dynamics control directional growth responses. Proc. Natl. Acad. Sci. USA *111*, 811–816.

Brunswik, H. (1924). Botanische Abhandlung (Jenna, Germany: Gustav Fischer).

Butty, A.C., Perrinjaquet, N., Petit, A., Jaquenoud, M., Segall, J.E., Hofmann, K., Zwahlen, C., and Peter, M. (2002). A positive feedback loop stabilizes the guanine-nucleotide exchange factor Cdc24 at sites of polarization. EMBO J. *21*, 1565–1576.

Caballero-Lima, D., Kaneva, I.N., Watton, S.P., Sudbery, P.E., and Craven, C.J. (2013). The spatial distribution of the exocyst and actin cortical patches is sufficient to organize hyphal tip growth. Eukaryot. Cell *12*, 998–1008.

Castro-Villarreal, P., Villada-Balbuena, A., Méndez-Alcaraz, J.M., Castañeda-Priego, R., and Estrada-Jiménez, S. (2014). A Brownian dynamics algorithm for colloids in curved manifolds. J. Chem. Phys. *140*, 214115.

Chapa-Y-Lazo, B., Lee, S., Regan, H., and Sudbery, P. (2011). The mating projections of *Saccharomyces cerevisiae* and *Candida albicans* show key characteristics of hyphal growth. Fungal Biol. *115*, 547–556.

Chiou, J.G., Balasubramanian, M.K., and Lew, D.J. (2017). Cell Polarity in Yeast. Annu. Rev. Cell Dev. Biol. *33*, 77–101.

Corvest, V., Bogliolo, S., Follette, P., Arkowitz, R.A., and Bassilana, M. (2013). Spatiotemporal regulation of Rho1 and Cdc42 activity during *Candida albicans* filamentous growth. Mol. Microbiol. *89*, 626–648.

Court, H., and Sudbery, P. (2007). Regulation of Cdc42 GTPase activity in the formation of hyphae in *Candida albicans*. Mol. Biol. Cell *18*, 265–281.

Crampin, H., Finley, K., Gerami-Nejad, M., Court, H., Gale, C., Berman, J., and Sudbery, P. (2005). *Candida albicans* hyphae have a Spitzenkörper that is distinct from the polarisome found in yeast and pseudohyphae. J. Cell Sci. *118*, 2935–2947.

Das, M., Wiley, D.J., Chen, X., Shah, K., and Verde, F. (2009). The conserved NDR kinase Orb6 controls polarized cell growth by spatial regulation of the small GTPase Cdc42. Curr. Biol. *19*, 1314–1319.

Davis, C.R., Richman, T.J., Deliduka, S.B., Blaisdell, J.O., Collins, C.C., and Johnson, D.I. (1998). Analysis of the mechanisms of action of the *Saccharomyces cerevisiae* dominant lethal cdc42G12V and dominant negative cdc42D118A mutations. J. Biol. Chem. *273*, 849–858.

Denker, A., Kröhnert, K., Bückers, J., Neher, E., and Rizzoli, S.O. (2011). The reserve pool of synaptic vesicles acts as a buffer for proteins involved in synaptic vesicle recycling. Proc. Natl. Acad. Sci. USA *108*, 17183–17188.

Dyer, J.M., Savage, N.S., Jin, M., Zyla, T.R., Elston, T.C., and Lew, D.J. (2013). Tracking shallow chemical gradients by actin-driven wandering of the polarization site. Curr. Biol. *23*, 32–41.

Ermak, D.L., and McCammon, J.A. (1978). Brownian dynamics with hydrodynamic interactions. J. Chem. Phys. *69*, 1352.

Foti, M., Audhya, A., and Emr, S.D. (2001). Sac1 lipid phosphatase and Stt4 phosphatidylinositol 4-kinase regulate a pool of phosphatidylinositol 4-phosphate that functions in the control of the actin cytoskeleton and vacuole morphology. Mol. Biol. Cell *12*, 2396–2411.

Freisinger, T., Klünder, B., Johnson, J., Müller, N., Pichler, G., Beck, G., Costanzo, M., Boone, C., Cerione, R.A., Frey, E., and Wedlich-Söldner, R. (2013). Establishment of a robust single axis of cell polarity by coupling multiple positive feedback loops. Nat. Commun. *4*, 1807.

Gallo Castro, D., and Martin, S.G. (2018). Differential GAP requirement for Cdc42-GTP polarization during proliferation and sexual reproduction. J. Cell Biol. *217*, 4215–4229.

Gerami-Nejad, M., Zacchi, L.F., McClellan, M., Matter, K., and Berman, J. (2013). Shuttle vectors for facile gap repair cloning and integration into a neutral locus in *Candida albicans*. Microbiology *159*, 565–579.

Ghosh, A., Samuel, J., and Sinha, S.A. (2012). A "Gaussian" for diffusion on the sphere. Europhys. Lett. *98*, 30003.

Ghugtyal, V., Garcia-Rodas, R., Seminara, A., Schaub, S., Bassilana, M., and Arkowitz, R.A. (2015). Phosphatidylinositol-4-phosphate-dependent membrane traffic is critical for fungal filamentous growth. Proc. Natl. Acad. Sci. USA *112*, 8644–8649.

Giese, W., Eigel, M., Westerheide, S., Engwer, C., and Klipp, E. (2015). Influence of cell shape, inhomogeneities and diffusion barriers in cell polarization models. Phys. Biol. *12*, 066014.

Girbardt, M. (1957). Der Spitzenkörper von *Polystictus versicolor* (L.). Planta *50*, 47–59.

Girbardt, M. (1969). Die Ultrastruktur der Apikalregion von Pilzhyphen. Protoplasma *67*, 413–441.

Gladfelter, A.S., Moskow, J.J., Zyla, T.R., and Lew, D.J. (2001). Isolation and characterization of effector-loop mutants of CDC42 in yeast. Mol. Biol. Cell *12*, 1239–1255.

Goryachev, A.B., and Leda, M. (2017). Cell Polarity: Spot-On Cdc42 Polarization Achieved on Demand. Curr. Biol. *27*, R810–R812.

Grove, S.N., and Bracker, C.E. (1970). Protoplasmic organization of hyphal tips among fungi: vesicles and Spitzenkörper. J. Bacteriol. *104*, 989–1009.

Gulli, M.P., Jaquenoud, M., Shimada, Y., Niederhäuser, G., Wiget, P., and Peter, M. (2000). Phosphorylation of the Cdc42 exchange factor Cdc24 by the PAK-like kinase Cla4 may regulate polarized growth in yeast. Mol. Cell *6*, 1155–1167.

Harris, S.D. (2019). Hyphal branching in filamentous fungi. Dev. Biol. *451*, 35–39.

Haupt, A., Ershov, D., and Minc, N. (2018). A Positive Feedback between Growth and Polarity Provides Directional Persistency and Flexibility to the Process of Tip Growth. Curr. Biol. *28*, 3342–3351e3.

Hope, H., Bogliolo, S., Arkowitz, R.A., and Bassilana, M. (2008). Activation of Rac1 by the guanine nucleotide exchange factor Dck1 is required for invasive filamentous growth in the pathogen *Candida albicans*. Mol. Biol. Cell *19*, 3638–3651.

Howell, A.S., Jin, M., Wu, C.F., Zyla, T.R., Elston, T.C., and Lew, D.J. (2012). Negative feedback enhances robustness in the yeast polarity establishment circuit. Cell *149*, 322–333.

Jaquenoud, M., and Peter, M. (2000). Gic2p may link activated Cdc42p to components involved in actin polarization, including Bni1p and Bud6p (Aip3p). Mol. Cell. Biol. *20*, 6244–6258.

Jones, L.A., and Sudbery, P.E. (2010). Spitzenkorper, exocyst, and polarisome components in *Candida albicans* hyphae show different patterns of localization and have distinct dynamic properties. Eukaryot. Cell *9*, 1455–1465.

Kelly, F.D., and Nurse, P. (2011). Spatial control of Cdc42 activation determines cell width in fission yeast. Mol. Biol. Cell *22*, 3801–3811.

Kennedy, M.J., Hughes, R.M., Peteya, L.A., Schwartz, J.W., Ehlers, M.D., and Tucker, C.L. (2010). Rapid blue-light-mediated induction of protein interactions in living cells. Nat. Methods *7*, 973–975.

Keppler-Ross, S., Noffz, C., and Dean, N. (2008). A new purple fluorescent color marker for genetic studies in *Saccharomyces cerevisiae* and *Candida albicans*. Genetics *179*, 705–710.

Kim, J., and Rose, M.D. (2015). Stable Pseudohyphal Growth in Budding Yeast Induced by Synergism between Septin Defects and Altered MAP-kinase Signaling. PLoS Genet. *11*, e1005684.

Köhli, M., Galati, V., Boudier, K., Roberson, R.W., and Philippsen, P. (2008). Growth-speed-correlated localization of exocyst and polarisome components in growth zones of *Ashbya gossypii* hyphal tips. J. Cell Sci. *121*, 3878–3889.

Kuo, C.C., Savage, N.S., Chen, H., Wu, C.F., Zyla, T.R., and Lew, D.J. (2014). Inhibitory GEF phosphorylation provides negative feedback in the yeast polarity circuit. Curr. Biol. *24*, 753–759.

Labbaoui, H., Bogliolo, S., Ghugtyal, V., Solis, N.V., Filler, S.G., Arkowitz, R.A., and Bassilana, M. (2017). Role of Arf GTPases in fungal morphogenesis and virulence. PLoS Pathog. *13*, e1006205.

Li, C.R., Lee, R.T., Wang, Y.M., Zheng, X.D., and Wang, Y. (2007). Candida albicans hyphal morphogenesis occurs in Sec3p-independent and Sec3p-dependent phases separated by septin ring formation. J. Cell Sci. *120*, 1898–1907.

Lichius, A., Goryachev, A.B., Fricker, M.D., Obara, B., Castro-Longoria, E., and Read, N.D. (2014). *CDC-42* and *RAC-1* regulate opposite chemotropisms in *Neurospora crassa*. J. Cell Sci. *127*, 1953–1965.

Löpez-Franco, R., and Bracker, C.E. (1996). Diversity and dynamics of the Spitzenkörper in growing hyphal tips of higher fungi. Protoplasma *195*, 90–111.

López-Franco, R., Howard, R.J., and Bracker, C.E. (1995). Satellite Spitzenkörper in growing hyphal tip. Protoplasma *188*, 85–103.

Luo, G., Zhang, J., and Guo, W. (2014). The role of Sec3p in secretory vesicle targeting and exocyst complex assembly. Mol. Biol. Cell *25*, 3813–3822.

Martin, S.G. (2015). Spontaneous cell polarization: Feedback control of Cdc42 GTPase breaks cellular symmetry. BioEssays *37*, 1193–1201.

Merrifield, C.J., Moss, S.E., Ballestrem, C., Imhof, B.A., Giese, G., Wunderlich, I., and Almers, W. (1999). Endocytic vesicles move at the tips of actin tails in cultured mast cells. Nat. Cell Biol. *1*, 72–74.

Milovanovic, D., and De Camilli, P. (2017). Synaptic Vesicle Clusters at Synapses: A Distinct Liquid Phase? Neuron *93*, 995–1002.

Mukherjee, K., Yang, X., Gerber, S.H., Kwon, H.B., Ho, A., Castillo, P.E., Liu, X., and Südhof, T.C. (2010). Piccolo and bassoon maintain synaptic vesicle clustering without directly participating in vesicle exocytosis. Proc. Natl. Acad. Sci. USA *107*, 6504–6509.

Mutavchiev, D.R., Leda, M., and Sawin, K.E. (2016). Remodeling of the Fission Yeast Cdc42 Cell-Polarity Module via the Sty1 p38 Stress-Activated Protein Kinase Pathway. Curr. Biol. *26*, 2921–2928.

Ortiz, D., Medkova, M., Walch-Solimena, C., and Novick, P. (2002). Ypt32 recruits the Sec4p guanine nucleotide exchange factor, Sec2p, to secretory vesicles; evidence for a Rab cascade in yeast. J. Cell Biol. *157*, 1005–1015.

Ottilie, S., Miller, P.J., Johnson, D.I., Creasy, C.L., Sells, M.A., Bagrodia, S., Forsburg, S.L., and Chernoff, J. (1995). Fission yeast *pak1+* encodes a protein kinase that interacts with Cdc42p and is involved in the control of cell polarity and mating. EMBO J. *14*, 5908–5919.

Ozbudak, E.M., Becskei, A., and van Oudenaarden, A. (2005). A system of counteracting feedback loops regulates Cdc42p activity during spontaneous cell polarization. Dev. Cell *9*, 565–571.

Pantazopoulou, A., Pinar, M., Xiang, X., and Peñalva, M.A. (2014). Maturation of late Golgi cisternae into RabE(RAB11) exocytic post-Golgi carriers visualized *in vivo*. Mol. Biol. Cell *25*, 2428–2443.

Peter, M., Neiman, A.M., Park, H.O., van Lohuizen, M., and Herskowitz, I. (1996). Functional analysis of the interaction between the small GTP binding protein Cdc42 and the Ste20 protein kinase in yeast. EMBO J. *15*, 7046–7059.

Pulver, R., Heisel, T., Gonia, S., Robins, R., Norton, J., Haynes, P., and Gale, C.A. (2013). Rsr1 focuses Cdc42 activity at hyphal tips and promotes maintenance of hyphal development in *Candida albicans*. Eukaryot. Cell *12*, 482–495.

Reijnst, P., Walther, A., and Wendland, J. (2011). Dual-colour fluorescence microscopy using yEmCherry-/GFP-tagging of eisosome components Pil1 and Lsp1 in *Candida albicans*. Yeast *28*, 331–338.

Reynaga-Peña, C.G., Gierz, G., and Bartnicki-Garcia, S. (1997). Analysis of the role of the Spitzenkörper in fungal morphogenesis by computer simulation of apical branching in *Aspergillus niger*. Proc. Natl. Acad. Sci. USA *94*, 9096–9101.

Rida, P.C., Nishikawa, A., Won, G.Y., and Dean, N. (2006). Yeast-to-hyphal transition triggers formin-dependent Golgi localization to the growing tip in *Candida albicans*. Mol. Biol. Cell *17*, 4364–4378.

Riquelme, M. (2013). Tip growth in filamentous fungi: a road trip to the apex. Annu. Rev. Microbiol. *67*, 587–609.

Riquelme, M., and Bartnicki-Garcia, S. (2004). Key differences between lateral and apical branching in hyphae of *Neurospora crassa*. Fungal Genet. Biol. *41*, 842–851.

Riquelme, M., and Sánchez-León, E. (2014). The Spitzenkörper: a choreographer of fungal growth and morphogenesis. Curr. Opin. Microbiol. *20*, 27–33.

Sánchez-León, E., Verdín, J., Freitag, M., Roberson, R.W., Bartnicki-Garcia, S., and Riquelme, M. (2011). Traffic of chitin synthase 1 (CHS-1) to the Spitzenkörper and developing septa in hyphae of *Neurospora crassa*: actin dependence and evidence of distinct microvesicle populations. Eukaryot. Cell *10*, 683–695.

Sánchez-León, E., Bowman, B., Seidel, C., Fischer, R., Novick, P., and Riquelme, M. (2015). The Rab GTPase YPT-1 associates with Golgi cisternae and Spitzenkörper microvesicles in *Neurospora crassa*. Mol. Microbiol. *95*, 472–490.

Smith, S.E., Rubinstein, B., Mendes Pinto, I., Slaughter, B.D., Unruh, J.R., and Li, R. (2013). Independence of symmetry breaking on Bem1-mediated autocatalytic activation of Cdc42. J. Cell Biol. *202*, 1091–1106.

Southwick, F.S., Li, W., Zhang, F., Zeile, W.L., and Purich, D.L. (2003). Actin-based endosome and phagosome rocketing in macrophages: activation by the secretagogue antagonists lanthanum and zinc. Cell Motil. Cytoskeleton *54*, 41–55.

Taunton, J., Rowning, B.A., Coughlin, M.L., Wu, M., Moon, R.T., Mitchison, T.J., and Larabell, C.A. (2000). Actin-dependent propulsion of endosomes and lysosomes by recruitment of N-WASP. J. Cell Biol. *148*, 519–530.

Umbach, D., and Jones, K.N. (2003). A Few Methods for Fitting Circles to Data. IEEE Trans. Instrum. Meas. *52*, 1881–1885.

Ushinsky, S.C., Harcus, D., Ash, J., Dignard, D., Marcil, A., Morchhauser, J., Thomas, D.Y., Whiteway, M., and Leberer, E. (2002). CDC42 is required for polarized growth in human pathogen *Candida albicans*. Eukaryot. Cell *1*, 95–104.

VandenBerg, A.L., Ibrahim, A.S., Edwards, J.E., Jr., Toenjes, K.A., and Johnson, D.I. (2004). Cdc42p GTPase regulates the budded-to-hyphal-form transition and expression of hypha-specific transcripts in *Candida albicans*. Eukaryot. Cell *3*, 724–734.

Vauchelles, R., Stalder, D., Botton, T., Arkowitz, R.A., and Bassilana, M. (2010). Rac1 dynamics in the human opportunistic fungal pathogen *Candida albicans*. PLoS ONE *5*, e15400.

Verdín, J., Bartnicki-Garcia, S., and Riquelme, M. (2009). Functional stratification of the Spitzenkörper of *Neurospora crassa*. Mol. Microbiol. *74*, 1044–1053.

Vernay, A., Schaub, S., Guillas, I., Bassilana, M., and Arkowitz, R.A. (2012). A steep phosphoinositide bis-phosphate gradient forms during fungal filamentous growth. J. Cell Biol. *198*, 711–730.

Virag, A., and Harris, S.D. (2006). The Spitzenkörper: a molecular perspective. Mycol. Res. *110*, 4–13.

Virag, A., Lee, M.P., Si, H., and Harris, S.D. (2007). Regulation of hyphal morphogenesis by *cdc42* and *rac1* homologues in *Aspergillus nidulans*. Mol. Microbiol. *66*, 1579–1596.

Wagner, W., Bielli, P., Wacha, S., and Ragnini-Wilson, A. (2002). Mlc1p promotes septum closure during cytokinesis via the IQ motifs of the vesicle motor Myo2p. EMBO J. *21*, 6397–6408.

Wakade, R. (2017). Role of the Rab GTPase, Ypt6, in the human fungal pathogen *Candida albicans*, PhD thesis.

Wakade, R., Labbaoui, H., Stalder, D., Arkowitz, R.A., and Bassilana, M. (2017). Overexpression of *YPT6* restores invasive filamentous growth and secretory vesicle clustering in a *Candida albicans* arl1 mutant. Small GTPases, 1–7.

Weiner, A., Orange, F., Lacas-Gervais, S., Rechav, K., Ghugtyal, V., Bassilana, M., and Arkowitz, R.A. (2019). On-site secretory vesicle delivery drives filamentous growth in the fungal pathogen *Candida albicans*. Cell. Microbiol. *21*, e12963.

Wilson, R.B., Davis, D., and Mitchell, A.P. (1999). Rapid hypothesis testing with *Candida albicans* through gene disruption with short homology regions. J. Bacteriol. *181*, 1868–1874.

Witte, K., Strickland, D., and Glotzer, M. (2017). Cell cycle entry triggers a switch between two modes of Cdc42 activation during yeast polarization. eLife *6*, e26722.

Woods, B., and Lew, D.J. (2019). Polarity establishment by Cdc42: Key roles for positive feedback and differential mobility. Small GTPases *10*, 130–137.

Wu, C.F., and Lew, D.J. (2013). Beyond symmetry-breaking: competition and negative feedback in GTPase regulation. Trends Cell Biol. *23*, 476–483.

Wu, C.F., Chiou, J.G., Minakova, M., Woods, B., Tsygankov, D., Zyla, T.R., Savage, N.S., Elston, T.C., and Lew, D.J. (2015). Role of competition between polarity sites in establishing a unique front. eLife *4*, e11611.

Zeng, G., Wang, Y.M., and Wang, Y. (2012). Cdc28-Cln3 phosphorylation of Sla1 regulates actin patch dynamics in different modes of fungal growth. Mol. Biol. Cell *23*, 3485–3497.

Zhang, C., and Konopka, J.B. (2010). A photostable green fluorescent protein variant for analysis of protein localization in *Candida albicans*. Eukaryot. Cell *9*, 224–226.

Zhang, X., Bi, E., Novick, P., Du, L., Kozminski, K.G., Lipschutz, J.H., and Guo, W. (2001). Cdc42 interacts with the exocyst and regulates polarized secretion. J. Biol. Chem. *276*, 46745–46750.

Zheng, Y., Bagrodia, S., and Cerione, R.A. (1994). Activation of phosphoinositide 3-kinase activity by Cdc42Hs binding to p85. J. Biol. Chem. *269*, 18727–18730.

STAR★METHODS

KEY RESOURCES TABLE

REAGENT or RESOURCE	SOURCE	IDENTIFIER
Chemicals, Peptides, and Recombinant Proteins		
Concanavalin A	Merck Millipore	Cat# 234567-1GM
Fetal bovine serum	Dutscher	Cat# P30-8500-500ml
Paraformaldehyde	Electorn Microscopy Sciences	Cat# RT 15710-16%
Alexa Fluor-568 phalloidin	ThermoFisher	Cat# A12380-300U
Experimental Models: Organisms/Strains		
C. albicans		N/A
ura3Δ::imm434/ura3Δ::imm434 his1Δ::hisG/his1Δ::hisG arg4Δ::hisG/arg4Δ::hisG	Wilson et al., 1999	BWP17
Same as BWP17 with *arl1Δ::HIS1/arl1Δ::URA3*	Labbaoui et al., 2017	PY2533
Same as BWP17 but with *RP10::ARG4-ACT1p-CibN-GFPγ-CtRac1-ADH1t*	This study	PY2935
Same as 2533 but with *MLC1/MLC1::MLC1-GFP-HIS1*	This study	PY3280
Same as PY2935 but with *NEUT5L::NAT1-TEF1p-Cry-mCh-Cdc42 [G12V,C188S]-TEF1t*	This study	PY3451
Same as BWP17 but with *NEUT5L::NAT1-TEF1p-Cry-GFPγ-Cdc42 [G12V,C188S]-TEF1t*	This study	PY3643
Same as PY3643 but with *NEUT5L::URA3-ADH1p-CibN-CtRac1-ACT1t*	This study	PY4059
Same as PY4059 but with *RP10::ARG4-ACT1p-CRIB-mCh-ADH1t*	This study	PY4172
Same as PY4059 but with *ABP1/ABP1::ABP1-mCh-HIS1*	This study	PY4175
Same as PY4059 but with *MLC1/MLC1::MLC1-mCh-HIS1*	This study	PY4268
Same as PY3643 but with *NEUT5L::URA3-ADH1p-CibN-CtRac1-ACT1t*	This study	PY4510
Same as PY4510 but with *RP10::ARG4-SEC4p-mSc-Sec4-ADH1t*	This study	PY4534
Same as PY4510 but with *ADH1/ADH1p::miRFP670-HIS1*	This study	PY4559
Same as PY4534 but with *MLC1/MLC1::MLC1-miRFP670-HIS1*	This study	PY4623
Same as PY4510 but with *MLC1/MLC1::MLC1-miRFP670-HIS1*	This study	PY4642
Same as PY4642 but with *RP10::ARG4-ADH1p-Sac1-mSc-ADH1t*	This study	PY4849
Same as PY4642 but with *RP10::ARG4-YPT31p-mCh-Ypt31-ADH1t*	This study	PY4949
Same as PY4642 but with *SEC7/SEC7::SEC7-3x-mSc-ARG4*	This study	PY4957
Same as PY4642 but with *SEC2/SEC2::SEC2-3x-mSc-ARG4*	This study	PY4963
Same as PY4642 but with *SEC3/SEC3::SEC3-3x-mSc-ARG4*	This study	PY4964
Same as BWP17 but with *NEUT5L::NAT1-TEF1p-Cry-GFPγ-Cdc42 [G12V,T35A,C188S]-TEF1t*	This study	PY5010
Same as PY5010 but with *NEUT5L::URA3-ADH1p-CibN-CtRac1-ACT1t*	This study	PY5058
Oligonucleotides		
cttctagtatacgcgtcttataatatagtacatttttttagctctcttaatttttctttttCTTGTACAAT TCATCCATACCATGGGTAATACC	This study	yeGFPCtRac1m
ttactagtttaattaagggcgcgccAATTGTTTTTGTATTTGTTGTTGTTGTTG	This study	CaAdh1pmAscIPacISpeI
ttactagtggcctgcaggGAGTGAAATTCTGGAAATCTGG	This study	CaAct1tpSpeISbfI
cttaattaaTTATAATATAGTACATTTTTTAGCTCTCTTAATTTTTCTTT TCTTtgatgaaccaccagctgaaccagctgaaccagctgaatcaaattcAATAT AATCAGTTTTTTCC	This study	CaCIBNlinkCtRac1mPacI
ttactagtttaattaagggcgcgccGATTGATTATGACTATAATG	This study	CaTEF1pmAscPacSpe
ttactagtggcctgcaggGCTAGTTGAATATTATGTAAGATCTG	This study	CaTEF1tpSpeISbfI
TTTAATTAAtgatgaaccaccagctgaaccagctgaaccagctgaatcaaattcAGCA GCACCAATCATAATTTGAGC	This study	CaCRYm-link-PacI

(*Continued on next page*)

Continued

REAGENT or RESOURCE	SOURCE	IDENTIFIER
ccagctgattatgttcctGcAgtttttgataattatgctgtaaccgt	This study	CaCdc42T35ApPstI
acggttacagcataattatcaaaaacTgCaggaacataatcagctgg	This study	CaCdc42T35AmPstI
Recombinant DNA		
CGTACGGACCGATGAATGGTGCTATTGGTGGTGATTTATTGTTAAA TTTTCCAGATATGTCAGTTTTAGAAAGACAAAGAGCACATTTGAAA TATTTAAATCCAACTTTTGATTCACCATTGGCTGGTTTTTTTGCTGA TTCATCAATGATTACTGGTGGTGAAATGGATTCATATTTGTCAACTG CTGGTTTAAATTTGCCAATGATGTATGGTGAAACTACTGTTGAAGG TGATTCAAGATTATCAATTTCACCAGAAACTACTTTGGGTACTGGT AATTTTAAAGCTGCTAAATTTGATACTGAAACTAAAGATTGTAATGA AGCTGCTAAAAAAATGACTATGAATAGAGATGATTTAGTTGAAGAA GGTGAAGAAGAAAAATCAAAAATTACTGAACAAAATAATGGTTCA ACTAAATCAATTAAAAAAATGAAACATAAAGCTAAAAAAGAAGA AAATAATTTTTCAAATGATTCATCAAAAGTTACTAAAGAATTGGA AAAAACTGATTATATTGGGAGCTCCGC	Genscript	CaCIBNRsrIISacI
CGCGGCGCGCCCATGAAAATGGATAAAAAAACTATTGTTTGGT TTAGAAGAGATTTAAGAATTGAAGATAATCCAGCTTTGGCTGC TGCTGCTCATGAAGGTTCAGTTTTTCCAGTTTTTATTTGGTGTC CAGAAGAAGAAGGTCAATTTTATCCAGGTAGAGCTTCAAGAT GGTGGATGAAACAATCATTAGCTCATTTGTCACAATCATTAAA AGCTTTGGGTTCAGATTTAACTTTGATTAAAACTCATAATACT ATTTCAGCTATTTTAGATTGTATTAGAGTTACTGGTGCTACTAA AGTTGTTTTTAATCATTTGTATGATCCAGTTTCATTAGTTAGA GATCATACTGTTAAAGAAAAATTGGTTGAAAGAGGTATTTC AGTTCAATCATATAATGGTGATTTATTGTATGAACCATGGGA AATTTATTGTGAAAAAGGTAAACCATTTACTTCATTTAATTCA TATTGGAAAAAATGTTTAGATATGTCAATTGAATCAGTTATGT TGCCACCACCATGGAGATTAATGCCAATTACTGCTGCTGCTG AAGCTATTTGGGCTTGTTCAATTGAAGAATTGGGTTTAGAAAA TGAAGCTGAAAAACCATCAAATGCTTTGTTAACTAGAGCTTGG TCACCAGGTTGGTCAAATGCTGATAAATTGTTAAATGAATTT ATTGAAAAACAATTGATTGATTATGCTAAAAATTCAAAAAAA GTTGTTGGTAATTCAACTTCATTATTGTCACCATATTTACATTT TGGTGAAATTTCAGTTAGACATGTTTTTCAATGTGCTAGAATG AAACAAATTATTTGGGCTAGAGATAAAAATTCAGAAGGTGAA GAATCAGCTGATTTGTTTTTAAGAGGTATTGGTTTGAGAGAAT ATTCAAGATATATTTGTTTTAATTTTCCATTTACTCATGAACAA TCATTATTGTCACATTTAAGATTTTTTCCATGGGATGCTGATGT TGATAAATTTAAAGCTTGGAGACAAGGTAGAACTGGTTATCCA TTGGTTGATGCTGGTATGAGAGAATTATGGGCTACTGGTTGGAT GCATAATAGAATTAGAGTTATTGTTTCATCATTTGCTGTTAAAT TTTTATTGTTACCATGGAAATGGGGTATGAAATATTTTTGGGA TACTTTGTTAGATGCTGATTTGGAATGTGATATTTTAGGTTGG CAATATATTTCAGGTTCAATTCCAGATGGTCATGAATTGGATA GATTAGATAATCCAGCTTTGCAAGGTGCTAAATATGATCCAG AAGGTGAATATATTAGACAATGGTTACCAGAATTGGCTAGATTA CCAACTGAATGGATTCATCATCCATGGGATGCTCCATTGACTGTT TTAAAAGCTTCAGGTGTTGAATTGGGTACTAATTATGCTAAACCAA TTGTTGATATTGATACTGCTAGAGAATTATTGGCTAAAGCTATTT CAAGAACTAGAGAAGCTCAAATTATGATTGGTGCTGCTTTAATTAAAGC	Genscript	CaCRYPHRAscIPacI
pFA-yemCh-HIS1 plasmid	Reijnst et al., 2011	N/A
pUC57 plasmid	Genscript	N/A
pDUP5 plasmid	Gerami-Nejad et al., 2013	N/A
pDUP3 plasmid	Gerami-Nejad et al., 2013	N/A
pEXPARG-ACT1p-CRIB-GFP-ADH1t	Corvest et al., 2013	N/A
pEXPARG-ACT1p-CRIB-mCh-ADH1t	This study	N/A
pEXPARG-ACT1p-CibN-GFP-ADH1t	This study	N/A

(*Continued on next page*)

Continued

REAGENT or RESOURCE	SOURCE	IDENTIFIER
pEXPARG-ACT1p-CibN-GFPγ-CtRac1-ADH1t	This study	N/A
pDUP5-ADH1p-(AscI-PacI-SpeI-SbfI)-ACT1t	This study	N/A
pDUP5-ADH1p-CibN-CtRac1-ACT1t	This study	N/A
pDUP3-TEF1-(AscI-PacI-SpeI-SbfI)-TEF1t	This study	N/A
pDUP3-TEF1-Cry2-(PacI-SpeI-SbfI)-TEF1t	This study	N/A
pDUP3-TEF1-Cry2-mCh-(SpeI-SbfI)-TEF1t	This study	N/A
pDUP3-TEF1-Cry2-mCh-Cdc42-TEF1t	This study	N/A
pDUP3-TEF1-Cry2-mCh-Cdc42[C188S]-TEF1t	This study	N/A
pDUP3-TEF1p-Cry2-mCh-Cdc42[G12V,C188S]-TEF1t	This study	N/A
pDUP3-TEF1p-Cry2-GFPγ-Cdc42[G12V,C188S]-TEF1t	This study	N/A
pDUP3-TEF1p-Cry2-GFPγ-Cdc42[G12V,T35A,C188S]-TEF1t	This study	N/A
pEXPARG-ADH1p-Sac1-GFP	Weiner et al., 2019	N/A
pEXPARG-ADH1p-Sac1-mSc	This study	N/A
Software and Algorithms		
ImageJ version 1.51 software	National Institutes of Health	ImageJ
Huygens Professional software version 18.04	Scientific-Volume Imaging	Huygens Professional
Volocity Software version 6.3	PerkinElmer	Volocity
MATLAB version 2017 software	MathWorks	MathWorks
GraphPad Prism 6 software	GraphPad	Prism
MetaMorph version 7.8.8.0 software	Molecular Devices	MetaMorph

LEAD CONTACT AND MATERIALS AVAILABILITY

Further information and requests for resources and reagents should be directed to and will be fulfilled by the Lead Contact, Robert A. Arkowitz (arkowitz@unice.fr).

EXPERIMENTAL MODEL AND SUBJECT DETAILS

Strains

C. albicans strain BWP17 was used, which is isogenic to SC5314 (Wilson et al., 1999). Derivatives of the BWP17 strain used in this study are listed in the Key Resources Table. Strains were grown in the dark in rich media (yeast extract peptone dextrose) at 30°C for all experiments and were incubated with an equal volume of fetal calf serum (FCS) at 37°C for induction of filamentous growth.

METHOD DETAILS

Strain and plasmid construction

Standard methods were used for *C. albicans* cell culture, molecular, and genetic manipulations as described (Hope et al., 2008). To generate optogenetic strains, the sequences encoding Cry2Phr and CibN (Kennedy et al., 2010) were codon optimized, synthesized and cloned into pUC57 (Genscript). CibN was cloned into pEXPARG-ACT1p-CRIB-GFP-ADH1t (Corvest et al., 2013) replacing CRIB using unique RsrII and SacI sites. GFPγ (Zhang and Konopka, 2010) was then amplified with a unique 5′ SacI site and 3′ primer encoding the Rac1 C-terminal plasma membrane targeting domain (KKRKIKRAKKCTIL) (Vauchelles et al., 2010) followed by a stop codon and MluI site. This GFPγ-CtRac1 was subsequently cloned into pEXPARG-ACT1p-CibN-GFP-ADH1t to replace GFP resulting in pEXPARG-ACT1p-CibN-GFPγ-CtRac1-ADH1t. An *ADH1* promoter and *ACT1* terminator were cloned into pDUP5 (Gerami-Nejad et al., 2013) using unique XmaI and NotI sites resulting in pDUP5-ADH1p-(AscI-PacI-SpeI-SbfI)-ACT1t. CibN was amplified with a unique 5′ AscI site and a 3′ 15 aa linker encoding EFDSAGSAGSAGGSS, followed by Rac1 C-terminal plasma membrane targeting domain and a PacI site and this was cloned into pDUP5-ADH1p-(AscI-PacI-SpeI-SbfI)-ACT1t resulting in pDUP5-ADH1p-CibN-CtRac1-ACT1t. The *TEF1* promoter and terminator were cloned into pDUP3 (Gerami-Nejad et al., 2013) using unique XmaI and NotI sites resulting in pDUP3-TEF1-(AscI-PacI-SpeI-SbfI)-TEF1t. Cry2 was cloned using unique AscI and PacI sites into pDUP3-TEF1-(AscI-PacI-SpeI-SbfI)-TEF1t resulting in pDUP3-TEF1-Cry2-(PacI-SpeI-SbfI)-TEF1t. The gene encoding yemCherry (Keppler-Ross et al., 2008) was then amplified with unique PacI and SpeI sites and cloned into pDUP3-TEF1-Cry2-(PacI-SpeI-SbfI)-TEF1t, resulting in pDUP3-TEF1-Cry2-mCh-(SpeI-SbfI)-TEF1t. Cdc42 or Cdc42[C188S] was

then cloned into the SpeI and SbfI sites resulting in pDUP3-TEF1-Cry2-mCh-Cdc42-TEF1t or pDUP3-TEF1-Cry2-mCh-Cdc42[C188S]-TEF1t. A mutation encoding the G12V alteration was generated by site directed mutagenesis resulting in pDUP3-TEF1p-Cry2-mCh-Cdc42[G12V,C188S]-TEF1t. Cry2 was amplified with 5′ AscI site and a linker encoding EFDSAGSAGSAGGSS followed by a PacI site. GFPγ was subsequently cloned into unique PacI and SpeI and finally Cdc42[G12V,C188S] was cloned into unique SpeI and SbfI sites resulting in pDUP3-TEF1p-Cry2-GFPγ-Cdc42[G12V,C188S]-TEF1t. For generation of Cdc42[G12V,T35A], a mutation encoding the T35A alteration was generated by site directed mutagenesis resulting in pDUP3-TEF1p-Cry2-GFPγ-Cdc42[G12V,T35A,C188S]-TEF1t. The CibN and Cry plasmids were linearized by either NgoMI or StuI and transformed into strains, which were subsequently grown in absence of light. The Abp1-mCh, Mlc1-mCh, Mlc1-miRFP670, Sec2-3x-mSc, Sec7-3x-mSc and Sec3-3x-mSc strains were generated by homologous recombination, using pFA-yemCh-HIS1 (Reijnst et al., 2011), pFA-miRFP670-HIS1, pFA-mSc-ARG4 and pFA-3x-mSc-ARG4 (to be described elsewhere). pEXPARG-SEC4p-mSc-Sec4 was constructed using 1311 bp *SEC4* promoter with unique NotI and RsrII sites, followed by codon optimized mSc (mSc; to be described elsewhere) with RsrII and AscI sites and *SEC4* ORF flanked by AscI and MluI sites. pEXPARG-YPT31p-mCh-Ypt31 was constructed in a similar fashion as pEXPARG-SEC4p-mSc-Sec4 (to be described elsewhere). The pEXPARG-ACT1p-CRIB-mCh plasmid was constructed by replacing GFP in pEXPARG-ACT1p-CRIB-GFP (Corvest et al., 2013) with yemCherry (Keppler-Ross et al., 2008). The pEXPARG-ADH1p-Sac1-mSc plasmid was constructed by replacing GFP in pEXPARG-ADH1p-Sac1-GFP (Weiner et al., 2019) with mSc. CRIB, Sec4, Ypt31 and Sac1 plasmids were linearized with StuI and transformed into optogenetic strains.

Microscopy

Cells were imaged as described using spinning-disk confocal microscopy (Bassilana et al., 2005; Ghugtyal et al., 2015) except that MetaMorph version 7.8.8.0 software (Molecular Devices) controlled the system and for experiments examining the actin cytoskeleton, Sec2, Sec3, Ypt31, Sac1 and Sec7, a PLANAPO TIRF 1.45 NA 100 × objective was used. A long pass LP540 filter was used in the transmission light path to prevent premature photoactivation. Exponentially growing cells (grown in the dark) were spotted on YEPD agar pads at 30°C or mixed with an equal volume of FCS and spotted on 25% (vol/vol) YEPD agar–75% (vol/vol) FCS pads at 37°C (Bassilana et al., 2005). Typically cells on FCS/agar pads were incubated for 30 – 40 min at 37°C prior to microscopy or, in order to have cells with short filaments, incubation was for 10-30 min. Photoactivation was accomplished by a 300 msec 488 nm (10% of a 25 mW diode-pumped solid-state laser) pulse, either 3 pulses 10 min apart or 6 pulses 5 min apart. For the analyses of filament extension rate with the Cdc42[G12V,T35A]$_{cyto}$ fusion, equal amounts of optogenetic strains expressing Cry2-GFP-Cdc42[G12V]$_{cyto}$ (also expressing cytoplasmic miRFP to identify it) or Cry2-GFP-Cdc42[G12V,T35A]$_{cyto}$ were mixed and imaged simultaneously. For imaging of fusions with weaker signals including Sec2, Sec3, Ypt31, Sac1 and Sec7, following incubation with FCS, cells were imaged on slides for 20-30 min. Images were acquired at indicated times, with 0.5 μm z sections (9 to 15) to capture the entire cell, except for Sec3-3x-mSc where 4 × 0.5 μm z sections were acquired every 5 min and Sac1-mSc where 33 × 0.2 μm z sections were acquired. For live cell imaging followed by actin visualization, cells were grown in a Concanavalin A treated (0.1 mg/mL) glass bottom microwell dish (MatTek Corporation). Following photoactivation, cells were fixed with 4% paraformaldehyde for 10 min, subsequently washed with PBS, and actin was labeled with Alexa Fluor-568 Phalloidin as described (Vernay et al., 2012). Fixed cells were imaged with 0.2 μm z sections (18 to 26). All images were deconvolved with Huygens Professional software version 18.04 (Scientific-Volume Imaging) with recommended settings and a signal to noise ratio of 5 to 10. Maximum or sum projections are shown and the latter was used for all quantitations. Image analysis was carried out with ImageJ (version 1.51) and Volocity Software version 6.3 (PerkinElmer). Objects were identified as previously described, using the SD mode in Volocity (Ghugtyal et al., 2015), where the selection is based on SDs above the mean intensity. Scale bar is 5 μm in all images except for actin images and zoom in of the region analyzed in FRAP images, where it is 1 μm. The data that support the findings of this study are available from the corresponding author upon request.

Fluorescence recovery after photo-bleaching (FRAP) analysis was performed on a Zeiss LSM880 inverted confocal microscope using a Plan-Apo 1.4 NA 63 × objective. Images were captured every 2 s at 0.1% maximum laser intensity. Bleaching was performed at 80% laser intensity using 10 × 0.5-1 msec photo-bleaching scans on circular area of 1-2 μm^2. Bleach areas were somewhat larger than the cluster of vesicles to account for the rapid movement of the new cluster. Photoactivation was accomplished with a 100W Hg excitation source and a 450 – 490 nm band pass filter using 2 × 1 s pulses of 25% intensity. The average signal intensity of an area somewhat smaller than the bleach ROI was determined (which was dynamic in the case of the new cluster) and was normalized to photobleaching during image acquisition, which was fit to a one phase decay regression: $Y = (Y_0 - \text{Plateau})(e^{-kx}) + \text{Plateau}$, of the average intensity elsewhere in the cell (using GraphPad Prism 6 software). Regression analysis to determine the FRAP $t_{1/2}$ was done using a one-phase exponential association function in GraphPad Prism 6 software as follows: $Y = Y_{max}(1-e^{-kx})$, where k is the rate constant and $t_{1/2}$ is $0.69/k$. Given the different sizes of the initial Spk and the dynamic vesicle cluster, it was not possible to determine the mobile fraction. In addition, as the signals were quite low, it was occasionally necessary to saturate the detector prior to bleaching.

Modeling

Data Analysis

Modeling was carried out using MATLAB version 2017 (MathWorks). To analyze movement of the vesicle clusters following photoactivation we first inferred their z-coordinate by projecting their x-y coordinate on the cortex of the mother cell, using z section information to assign the cluster to the top or bottom hemi-sphere. To this end, we approximated the shape of the mother cell as a sphere.

To determine the sphere that best approximates the mother cell, we started from a two dimensional projection of the cell shape; discarding the filament and keeping the mother cell. We then used the Average of Intersections Method (Ghosh et al., 2012) to determine the optimal circle that best approximates the projected shape of the mother cell. Briefly, we grouped the ensemble of points on the mother cell cortex into triplets and traced all circles passing through the triplets. We obtained the center of the optimal circle by averaging over all the centers and the radius was defined as the average distance between the center and all the points. To minimize instabilities, we choose triplets of points as far away from each other as possible. Mother cells are spherical to a good approximation: the distance of the points on the mother cell cortex to the optimum circle range from 0.9% to 3.4% of the radius. The colatitude θ (Figure 7D) is defined relative to the North pole, which is the initial position of the vesicle cluster is aligned to. Note that there is little variation in the statistics when the position of the cluster at any other time point, is aligned to the North pole, corroborating that the dynamics is not dependent on the initial conditions and effectively does not depend on time.

Simulations of diffusion

We obtained replicas of the experimental dataset for purely diffusive dynamics using the algorithm developed by Ermak and McCammon (1978), with an additional term to keep the process on the surface of the sphere (Castro-Villarreal et al., 2014). To this end, we let the cluster start at the initial location of the real cluster on the cell cortex. We then defined a small time step, over which the cluster takes a step in a random direction and we applied a force that keeps it on the spherical representation of the mother cell. We use

$\mathbf{x}_i(t + dt) = \mathbf{x}_i(t) + D\,\mathbf{f}_j(t)\,dt + \delta\mathbf{x}_i$ where D is the diffusivity, $\delta\mathbf{x}_i$ are random variables with multivariate statistics $\langle \delta\mathbf{x}_i \delta\mathbf{x}_j \rangle = 2Dt$; $\mathbf{f}_i$ is the term keeping the cluster on the sphere, $\mathbf{f}_i = -k(r_i - R)\mathbf{n}_i$, R is the radius of the sphere, k quantifies the strength of the force, r_i is the distance of the cluster from the center and $\mathbf{n}_i$ is the unit vector normal to the surface of the sphere. We used D = 1.4 μm^2/min, which is within the range of variation of typical diffusivities in cells (Giese et al., 2015) and k = 1000 μm^{-2}, dt = 0.5 × 10^{-5} min. We recorded the position of the walkers every 2 × 10^5 time steps, corresponding to 1 min (which is the time between subsequent experimental acquisitions).

The theoretical prediction for diffusion on a sphere can be written in the form of a series of Legendre polynomials and reduced to the simple form

$P(\theta,\tau) \sim 1/\tau\theta \exp(-\theta^2/(2\tau))$ at small τ (Umbach and Jones, 2003), where $\tau = 2Dt/R^2$, θ is the colatitude, D is diffusivity and R is the radius of the sphere. Predictions for diffusion at short and long times (Figures S7A–S7C) are obtained as integrals of the full distribution over the desired time interval (Figures S7B and S7C; t < 10 min, t > 15 min).

Sample sizes

For Figures S7B and S7C, the data have been divided into early (first 10 min after initial photo-activation) and late (times later than 15 minutes after initial photoactivation). These time windows have been chosen empirically to ensure that the two classes contain a comparable number of data points.

QUANTIFICATION AND STATISTICAL ANALYSIS

Image quantification was carried out with ImageJ (version 1.51) and Volocity Software version 6.3 (PerkinElmer). The number of experiments and cells analyzed and means with standard deviation are indicated in Figure Legends (Figure S4E, standard error of the mean is shown). Data were compared by unpaired t test using GraphPad Prism (v. 6) software or Kolmogorov–Smirnov test, with all *p* values indicated in Figure Legends.

DATA AND CODE AVAILABILITY

The raw data and code that support the findings of this study are available from the corresponding author upon request.